The Astrophysical Journal, 946:116 (18pp), 2023 April 1 https://doi.org/10.3847/1538-4357/acbd4d

Galaxy and Mass Assembly (GAMA): Low-redshift Quasars and Inactive Galaxies Have Similar Neighbors

Maria B. Stone[1,2], Clare F. Wethers[3], Roberto de Propris[2,4], Jari Kotilainen[1,2], Nischal Acharya[5], Benne W. Holwerda[6], Jonathan Loveday[7], and Steven Phillipps[8]
[1] Department of Physics and Astronomy, Vesilinnantie 5, FI-20014 University of Turku, Finland; mbstone12@gmail.com
[2] Finnish Centre for Astronomy with ESO (FINCA), Vesilinnantie 5, FI-20014 University of Turku, Finland
[3] Department of Space, Earth and Environment, Chalmers University of Technology, Onsala Space Observatory, SE-439 92, Onsala, Sweden
[4] Department of Physics and Astronomy. Botswana International University of Science and Technology (BIUST), Private Bag 16, Palapye, Botswana
[5] Donostia International Physics Center (DIPC), Paseo Manuel de Lardizabal 4, E-20018 Donostia-San Sebastian, Spain
[6] Department of Physics and Astronomy, University of Louisville, Natural Science Building 102, Louisville, KY, 40292, USA
[7] Astronomy Centre, University of Sussex, Falmer, Brighton BN1 9QH, UK
[8] Astrophysics Group, School of Physics, University of Bristol, Tyndall Avenue, Bristol BS8 1TL, UK
Received 2022 October 24; revised 2023 February 7; accepted 2023 February 18; published 2023 April 7

Abstract

We explore the properties of galaxies in the proximity (within a ∼2 Mpc radius sphere) of Type I quasars at $0.1 < z < 0.35$, to check whether and how an active galaxy influences the properties of its neighbors. We further compare these with the properties of neighbors around inactive galaxies of the same mass and redshift within the same volume of space, using the Galaxy and Mass Assembly spectroscopic survey. Our observations reveal no significant difference in properties such as the number of neighbors, morphologies, stellar mass, star formation rates, and star formation history between the neighbors of quasars and those of the comparison sample. This implies that quasar activity in a host galaxy does not significantly affect its neighbors (e.g., via interactions with the jets). Our results suggest that quasar host galaxies do not strongly differ from the average galaxy within the specified mass and redshift range. Additionally, the implication of the relatively minor importance of the environmental effect on and from quasars is that nuclear activity is more likely triggered by internal and secular processes.

Unified Astronomy Thesaurus concepts: Galaxy evolution (594); Quasars (1319); Active galaxies (17); Active galactic nuclei (16); Star formation (1569); Galaxy environments (2029); Galaxies (573); Companion galaxies (290); Supermassive black holes (1663); Galaxy mergers (608)

1. Introduction

Active galactic nuclei (AGNs) are supermassive black holes (SMBHs) observed in the process of accreting matter (e.g., Lynden-Bell 1969). Although SMBHs are likely present within the centers of all massive galaxies (Kormendy & Ho 2013, and references therein), it is still unclear how the activity is switched on or off. Driving gas and dust to galaxy centers to feed the SMBH is found to be difficult (e.g., Alexander & Hickox 2012); however numerical simulations show that gravitational torques during galaxy mergers and interactions are able to produce inflows of gas toward the galactic central regions (Barnes & Hernquist 1991; Newton & Kay 2013; Wurster & Thacker 2013; Blumenthal & Barnes 2018) and feed central SMBHs, triggering AGN activity (Sanders et al. 1988; Debuhr et al. 2011). Pericenter passes among galaxy pairs also correlate with peaks in both SMBH and stellar activity (Gabor et al. 2016). Secular evolution instead occurs when instabilities in galaxies drive gas inward and fuel the SMBH (Shlosman et al. 1989; Hopkins & Quataert 2010). Such secular processes may involve bar instabilities or spiral arms (e.g., Villforth et al. 2019; Smethurst et al. 2021). This also may trigger star formation (SF) and AGN activity.

Observational evidence regarding which one is the dominant mechanism remains ambiguous. Some studies find no significant evidence that the hosts of AGN are more likely to be involved in mergers, compared to samples of inactive galaxies with the same luminosity and redshift (Cisternas et al. 2011; Villforth et al. 2017; Marian et al. 2020; Holwerda et al. 2021), while others make the opposite claim, particularly for IR-selected AGN (Fan et al. 2016; Goulding et al. 2018; Zhuang & Ho 2022). It is possible that the merger mechanism is only important for the more luminous AGN (e.g., $L_{\rm bol} > 10^{45}$ erg s^{-1}, Treister et al. 2012), or depends on other properties such as luminosity, obscuration, and age (Hopkins et al. 2006; Hopkins & Hernquist 2006; Hopkins & Quataert 2010).

As the environment may affect the properties of AGN hosts through mergers and interactions (e.g., Kormendy et al. 2009; Lietzen et al. 2011; Porqueres et al. 2018; Wethers et al. 2022, hereafter W22), so may AGN also affect the properties of their immediate neighbors (e.g., Gunn 1979; Silk & Rees 1998; Dashyan et al. 2019; Martín-Navarro et al. 2020; Martin-Navarro et al. 2021; Zana et al. 2022), e.g., through jets up to Mpc scales (Schaye et al. 2010; Padovani 2016; Blandford et al. 2019). Therefore the properties of galaxies neighboring AGN may provide information on the influence of the AGN on its neighbors, as well as on the triggering mechanism and the characteristics of AGN hosts: as an example, if most companion galaxies appear to be early-type, it would be more likely for the AGN host to be an early-type galaxy as well (Dressler 1980).

It is broadly accepted that feedback from the SMBH activity affects the properties of host galaxies, such as their star

formation rate (SFR; Sánchez et al. 2018; Martin-Navarro et al. 2022). The AGN activity, however, also influences the processes and the recycling of elements in the circumgalactic medium (Tumlinson et al. 2017) and beyond, potentially influencing the properties of the galaxies around the AGN (Molnár et al. 2017; Martin-Navarro et al. 2019). The influence may depend on quasar host luminosity, mass, SFR, group density, redshift, satellite distance from the quasar, as well as quasar type (obscured or unobscured). A recent study of an archival sample of satellite galaxies of brightest group galaxies (more likely to host or have hosted a quasar, as also shown by W22) by Martin-Navarro et al. (2021) showed that galaxies were less quenched along the direction of the quasar jets, where they excavate the intragroup medium and make ram stripping less effective.

There have been claims that regions around AGN are overdense (Serber et al. 2006; Strand et al. 2008; Zhang et al. 2013), but these lack comparison samples around inactive galaxies. Most previous studies have concentrated on finding samples of companion galaxies (e.g., Villarroel 2012; Karhunen et al. 2014; Yue et al. 2019) to measure the merger rate around AGN. Coldwell & Lambas (2003, 2006) claim that there is an excess of star-forming disk galaxies within 1 Mpc of AGN. Modest evidence was further found for star-forming neighbors of low-redshift quasars (Bettoni et al. 2017, 2023; Stone et al. 2021, hereafter S21).

In order to properly compare the environments of quasar host galaxies with those of currently inactive objects, we need large spectroscopic samples, allowing us to select both quasars and normal galaxies in the same manner and therefore isolate the influence of the environment on quasars and vice versa. Galaxy and Mass Assembly (GAMA Driver et al. 2011; Liske et al. 2015; Baldry et al. 2018; Driver et al. 2022) is a highly complete spectroscopic survey for redshifts of $z < 0.4$. Additionally, the GAMA data set includes multiwavelength photometry (over 22 bands) and rich ancillary information (derived quantities such as stellar mass, specific SF).

The GAMA survey is ideally suited for statistical studies of neighborhoods of low-redshift galaxies at the sub-Mpc scale, since it covers a sufficiently large area, and its redshift measurements are reliable, spatially uniform, and highly complete, and extend to the galaxies with faint fluxes. The observational methodology and instrument configurations of GAMA survey provide high target density, thus making it highly complete even for close pairs (De Propris et al. 2014; Robotham et al. 2014). In particular, GAMA survey is designed to have multiple passes to the same region; thus it is not affected by fiber placement restrictions, which consequently ensures the redshift completeness of close pairs (Driver et al. 2011; Robotham et al. 2014; Liske et al. 2015). The "close pair" definition is based on magnitude-redshift space-based samples to ensure completeness, as shown in GAMA survey-based study of close pair fractions at low redshift (De Propris et al. 2014). The survey extends down to a magnitude limit of Sloan Digital Sky Survey (SDSS) $r < 19.8$ mag. It is r-selected, so even sources with dust obscuration are less likely to be missed by the survey.

W22 exploited the GAMA data, showing that the quasar host galaxies, compared to a sample of inactive galaxies matched in mass and redshift, did not occupy significantly different environments. The high completeness and extensive information derived for GAMA targets allows us to consider the opposite question—whether the properties of galaxies in the neighborhood of quasars are affected by the proximity of quasar host galaxies.

Here we use GAMA data to expand on the work by S21, Bettoni et al. (2017, 2023), on low-redshift ($z < 0.5$) quasar environments in the Sloan Digital Sky Survey (SDSS Ahumada et al. 2020) Stripe82 region (Annis et al. 2014). In these studies, long slits were placed on galaxies within several hundred kiloparsecs of the projected distance of quasars, to identify physically associated companion galaxies (at the same redshift) and to determine their properties. Similarly, here, we identify spectroscopically confirmed companion galaxies contained within a fixed comoving volume (radius ∼2 Mpc) for each quasar from the independent sample of quasars defined in W22, and compare the properties of these neighboring galaxies against a comparison sample of neighboring galaxies around inactive galaxies whose properties (stellar mass and redshift) are matched to those of the quasar hosts.

The outline of the paper is as follows. The quasar sample, the comparison galaxy samples, and the identification of neighboring galaxies from the GAMA survey are described in Section 2. The results of the comparison between the neighbors around quasars and inactive galaxies are presented in Section 3 and discussed in Section 4. We summarize in Section 5. The analysis is performed assuming the flat Λ cold dark matter (ΛCDM) cosmology model with the following parameters: the matter density parameter $\Omega_M = 0.3$, the cosmological constant $\Omega_\Lambda = 0.7$, the Hubble constant $H_0 = 70$ km s^{-1} Mpc^{-1} (Planck Collaboration et al. 2020).

2. DATA

This work is based on the whole sample of 205 Type I quasars at $0.1 < z < 0.35$ as defined in W22. In short, these quasars were selected from version 4 of the Large Quasar Astrometric Catalog (LQAC4; Gattano et al. 2018), constrained to the GAMA equatorial regions, and restricted to be above the GAMA survey depth ($r < 19.8$).

We next used GAMA to select a comparison sample of inactive galaxies matched in redshift and stellar mass to our sample of quasar hosts, following the method used in W22. We created 200 such *Monte Carlo* realizations, which is sufficiently high to have robust statistical comparison. Each realization contains 205 matched inactive galaxies, matching the number of quasars in our sample. The redshift and stellar mass distributions of the quasar sample and the matched inactive galaxies (from all realizations combined) show that the selected comparison galaxies are closely matched to quasars (Figure 1).

The luminosity distribution of the quasar sample is shown in Figure 2, using the available absolute magnitudes reported in the LQAC4 catalog (Ochsenbein et al. 2000; Gattano et al. 2018). Note that the luminosities here include contributions from the nuclear activity as well as from the host galaxy. The median value for absolute B magnitude is $-21.50^{-20.81}_{-22.08}$ (the uncertainty is reported as lower and upper quartiles). The median value for absolute I magnitude is $-21.42^{-20.84}_{-21.98}$. As expected, our sample based on LQAC4 and GAMA consists of relatively low-luminosity quasars, i.e., the typical objects occupying a specified volume of space.

The median log(SFR) estimate for quasars (comparison galaxies) is 0.90 (−0.12) $M_\odot$ yr^{-1}; however the contribution of AGN is not accounted for by the version of MAGPHYS used

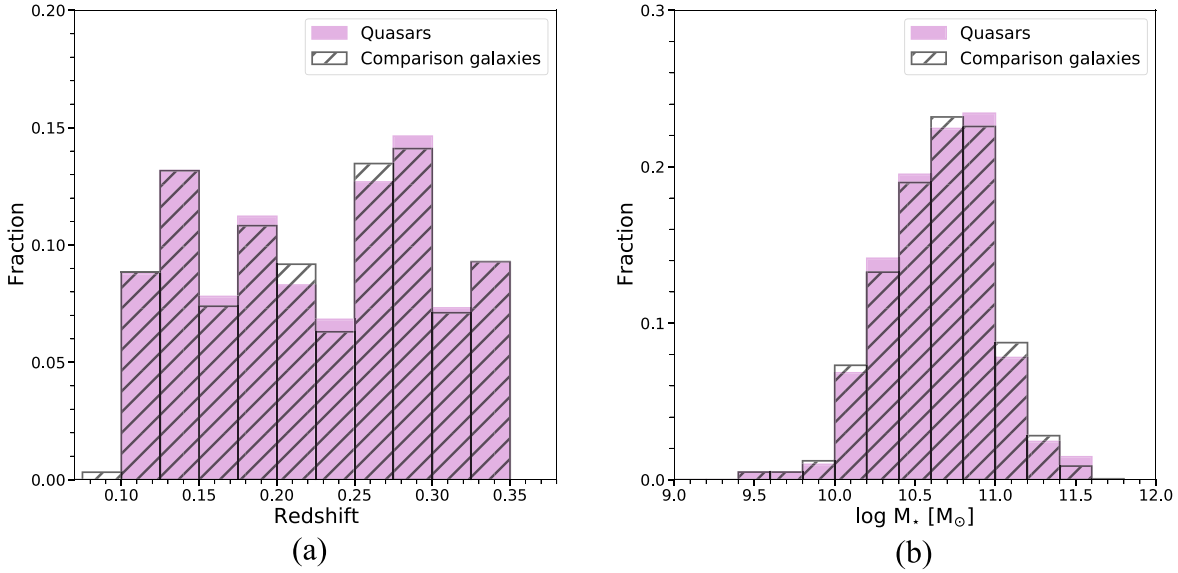

Figure 1. Distributions of (a) redshift and (b) stellar mass for quasars and for the matched inactive galaxies.

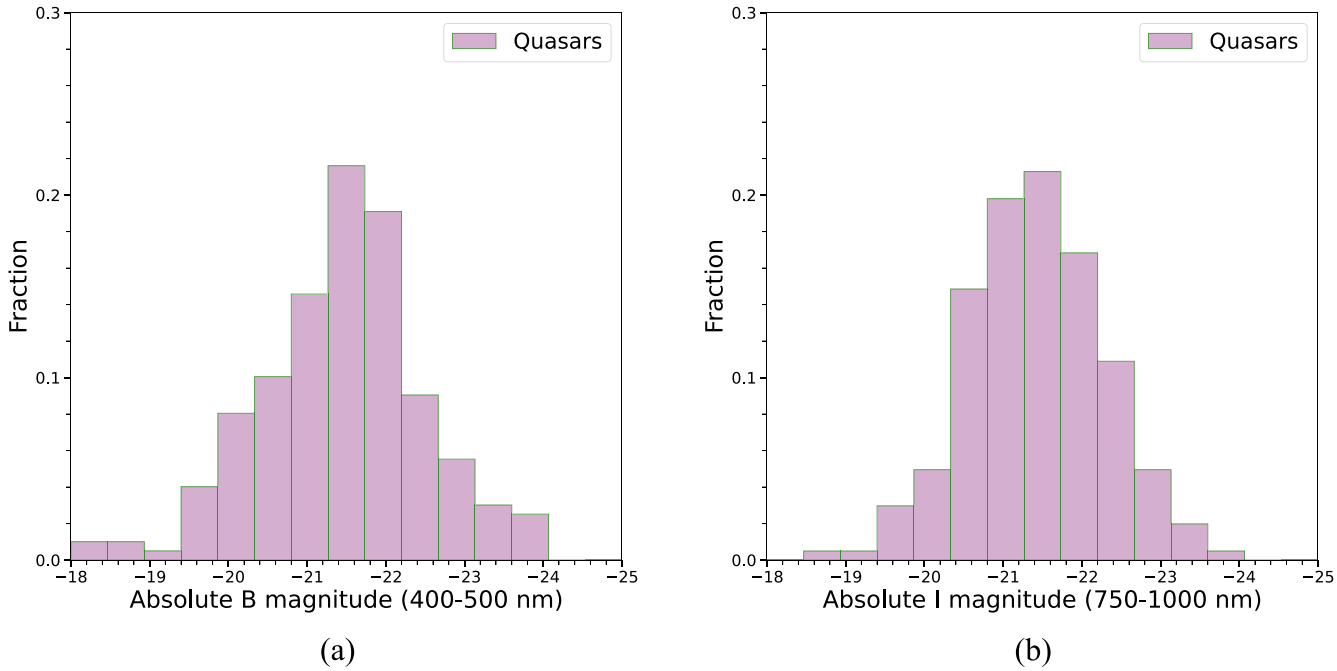

Figure 2. Distributions of absolute magnitudes in *B* and *I* for LQAC4 quasars in this sample.

in the GAMA survey, and these estimates have to be taken under advisement. The range of log(SFR) for quasars is −0.36 −2.22 $M_{\odot}$ yr^{-1}, while for comparison galaxies, −3.64−2.22 $M_{\odot}$ yr^{-1}. For the purpose of comparison, we show few example images of quasar host galaxies and comparison galaxies in Figures 3 and 4 (Ahn et al. 2014).

Next, to find the neighbors for each quasar, we select galaxies within a fixed comoving sphere of radius (R ∼ 1.8 Mpc) using the positions and redshifts provided by the latest GAMA catalog (SpecCat data management unit, hereafter DMU, Baldry et al. 2014, 2018; Liske et al. 2015). This radius corresponds to the characteristic radius R_{200} (Carlberg et al. 1996, 1997) for a system with an internal velocity dispersion of 700 km s^{-1}, which is equivalent to a relatively poor cluster or a rich group, i.e., the typical environment in which most galaxies tend to reside, including the AGN host galaxies in W22. A similar comoving volume was surveyed around each of the comparison galaxies. The GAMA survey redshifts have median velocity uncertainty of 33 km s^{-1} (Baldry et al. 2014).

We use this sample to investigate the close environment of AGN hosts and compare it to that of inactive galaxies. Additionally, we use derived quantities from the GAMA survey to compare the properties of neighbors for both AGN host galaxies and matched inactive galaxies by performing the two-sample Kolmogorov–Smirnov (KS) test, as in W22, implemented with the scipy.stats.ks_2samp routine. Table 1 shows the derived quantities used and the appropriate GAMA DMU employed, with reference to the published description in

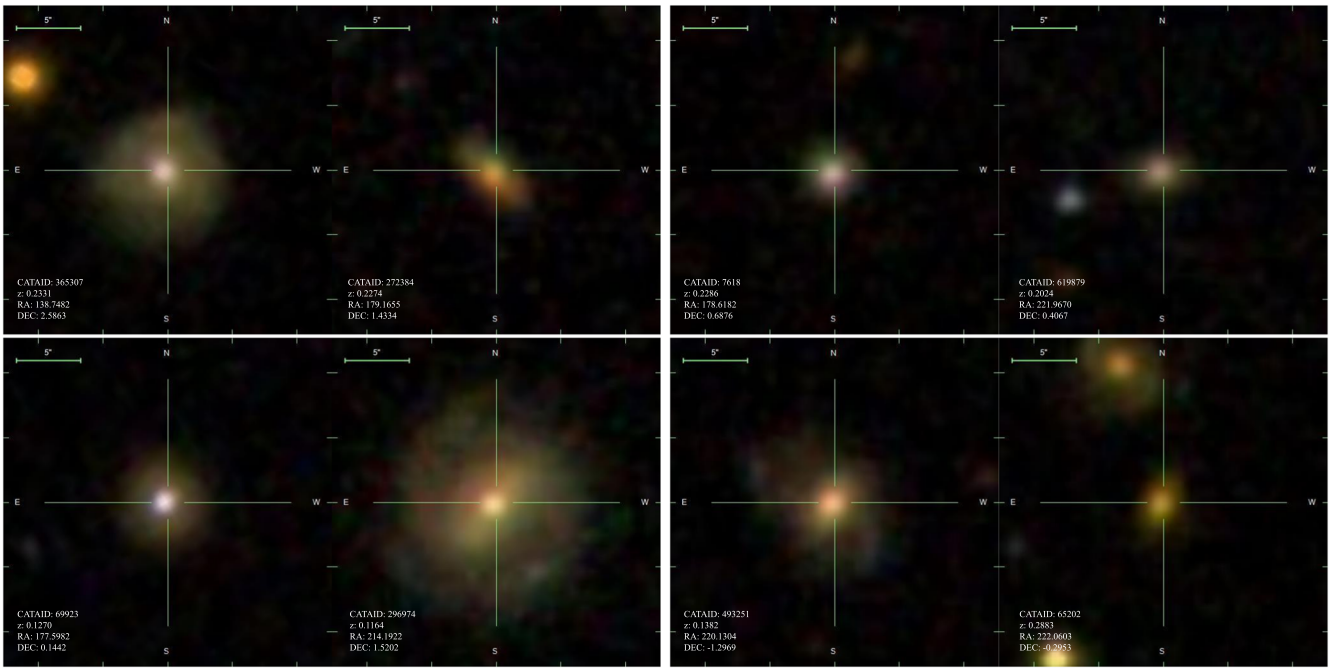

Figure 3. Quasar host galaxy examples in our sample.

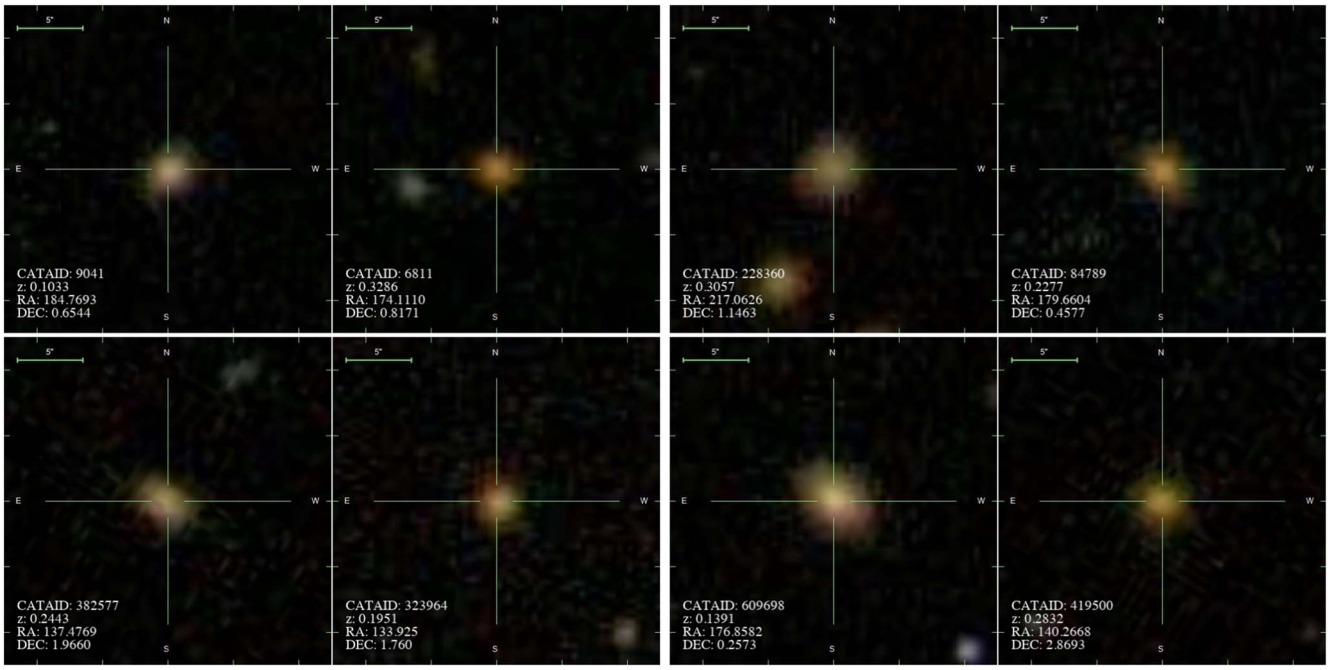

Figure 4. Comparison galaxy examples.

each case. Because the KS test is not as sensitive to the wings of the distribution, a two-sample Anderson–Darling (AD) test was also performed using the scipy.stats.anderson_ksamp package.

2.1. GAMA Ancillary Products

The various galaxy properties have been derived by the GAMA collaboration as ancillary information. These data are included in the survey as Sérsic photometry, LambdarPhotometry, and MagPhys DMUs. In this section, we briefly describe how GAMA derived these properties. We refer the reader to the references for further details.

The colors of neighbors are computed using the absolute (AB) system magnitudes supplied by the GAMA Lambdar-Photometry DMU (Driver et al. 2016; Wright et al. 2016). The deblended matched aperture photometry is calculated using the LAMBDAR code ("lambda adaptive multiband deblending algorithm in R"). We used SDSS $u-r$, $g-r$, and Galaxy Evolution Explorer (GALEX) near-UV (NUV)−SDSS r colors (Martin et al. 2005). We exploited the following individual filter catalogs: LambdarSDSSu (v01), LambdarSDSSg (v01), LambdarSDSSr (v01), and LambdarGALEXNUV (v01) to

Table 1
KS and AD Test Results

Property	Units	Statistic D_{KS} (A_k)	p-value p_{KS} (p_{AD})	Figure	References
DISTANCE					
Comoving separation from quasar (comparison galaxy)	Mpc	0.06 (−0.5)	0.84 (0.25)	Figure 6	
MORPHOLOGY from `Sérsic photometry` DMU					(1), (4), (5)
Sérsic index (n)	⋯	0.15 (−0.4)	0.12 (0.25)	Figure 11	
COLORS from `LambdarPhotometry`DMU					(2), (6)
SDSS $u-r$	⋯	0.08 (−0.6)	0.80 (0.25)	Figure 12(a)	
SDSS $g-r$	⋯	0.10 (−0.5)	0.54 (0.25)	Figure 13(a)	
GALEX NUV-SDSS r	⋯	0.09 (−0.7)	0.77 (0.25)	Figure 14(a)	
SFH and PHYSICAL PARAMETERS from `MagPhys` DMU					(1), (3)
SFR	$M_\odot$ yr^{-1}	0.06 (−0.9)	0.96 (0.25)	Figure 15(a)	
SSFR	yr^{-1}	0.07 (−0.7)	0.89 (0.25)	Figure 15(b)	
SFR_{ave} over the last 10^7 yr	$M_\odot$ yr^{-1}	0.07 (−0.2)	0.88 (0.25)	Figure 16(a)	
SFR_{ave} over the last 10^8 yr	$M_\odot$ yr^{-1}	0.07 (−0.7)	0.86 (0.25)	Figure 16(b)	
SFR_{ave} over the last 10^9 yr	$M_\odot$ yr^{-1}	0.09 (−0.5)	0.67 (0.25)	Figure 16(c)	
SFR_{ave} over the last 2×10^9 yr	$M_\odot$ yr^{-1}	0.11 (−0.1)	0.37 (0.25)	Figure 16(d)	
SF timescale	Gyr^{-1}	0.08 (−0.8)	0.73 (0.25)	Figure 17(a)	
Time since the last burst of SF ended	dex (yr)	0.09 (−0.6)	0.64 (0.25)	Figure 17(b)	
Total $M_\star$ ever formed (integral of the SFR)	$M_\odot$	0.12 (0.1)	0.32 (0.25)	Figure 18(a)	
Total mass of dust	$M_\odot$	0.05 (−0.9)	0.99 (0.25)	Figure 18(b)	
Fraction of mass formed in bursts over the last 10^7 yr	⋯	0.04 (18.9)	0.99 (0.001)	Figure 19(a)	
Fraction of mass formed in bursts over the last 10^8 yr	⋯	0.04 (6.0)	0.99 (0.001)	Figure 19(b)	
Fraction of mass formed in bursts over the last 10^9 yr	⋯	0.08 (−0.3)	0.84 (0.25)	Figure 19(c)	
Fraction of mass formed in bursts over the last 2×10^9 yr	⋯	0.15 (0.4)	0.12 (0.22)	Figure 19(d)	
Age of the oldest stars in the galaxy	dex (yr)	0.07 (−0.9)	0.88 (0.25)	Figure 20(a)	
Metallicity	$Z_\odot$	0.12 (−0.2)	0.33 (0.25)	Figure 20(b)	

Note. KS and AD test comparisons between the spectroscopically confirmed neighbors of quasars and matched inactive galaxies. D_{KS} is the calculated KS test statistic. A_k is the calculated AD test statistic for $k=2$ samples. The AD test statistic and p-values are in parentheses. The p-values of the AD test are capped at 25%. For MagPhys DMU, we used the latest internal version.
References. (1) Baldry et al. (2018); (2) Driver et al. (2016); (3) Driver et al. (2018); (4) Hill et al. (2011); (5) Kelvin et al. (2012); (6) Wright et al. (2016).

retrieve the reported AB magnitudes of final deblended flux and their associated errors.

To describe the morphologies, the Sérsic indices reported are surface brightness distribution fits to a single component Sérsic profile (Sérsic 1968) in the SDSS r band (Sérsic photometry DMU, version 9; Hill et al. 2011; Kelvin et al. 2012; Baldry et al. 2018). The Sérsic index value and its associated error are retrieved from the SérsicCatSDSS catalog. The fit is produced by the SIGMA tool ("structural investigation of galaxies via model analysis," v1, Kelvin et al. 2012) based on the GALFIT two-dimensional fitting algorithm (Peng et al. 2002, 2010). The code performs a nonlinear least-squares fit and calculates the goodness of fit using the normalized χ^2 computation technique, estimating the uncertainty in each pixel based on its Poisson error.

This study makes use of the physical stellar population parameters for galaxies provided by the MagPhys table within the MagPhys spectral energy distribution (SED) DMU (Baldry et al. 2018; Driver et al. 2018, latest internal version). The parameters are derived through the execution of the MAGPHYS code (multiwavelength analysis of galaxy physical properties) for fitting the SED of a galaxy (da Cunha et al. 2008; da Cunha & Charlot 2011). MAGPHYS assumes energy conservation, which relies on the Bruzual & Charlot (2003) models, does not include AGN emission, and is based on Bayesian method. MAGPHYS SED fitting results are in general agreement with similar codes in the literature (Hayward & Smith 2015; Hunt et al. 2019). It was applied to the 21 band GAMA photometry catalog (LambdarCat, v01; Wright et al. 2016; Driver et al. 2018) spanning the far-ultraviolet (FUV) to far-infrared (FIR) wavelength regime.

We focus on the galaxy-wide physical parameters pertaining to the stars: stellar mass estimates (separate from the stellar mass estimates from Taylor et al. 2011; see Baldry et al. 2018 for a discussion comparing the two), SFR estimates over different timescales, specific SFR (sSFR), metallicity, age of the oldest stars in the galaxy, SF timescale, fraction of stellar mass formed in bursts over various timescales. Figure 5 shows the results of this procedure for one example companion galaxy and its SDSS image (Ahn et al. 2014).

MAGPHYS estimates the parameters of stellar populations (age, metallicity, SF metrics) and the interstellar medium by comparing multiband photometry against a large library of stellar templates and dust emission templates in the mid-infrared and FIR. This returns best-fit and median estimates for the sought parameters. In this work, we used the best-fit values for the SFR, sSFR, stellar mass, and dust mass, while for the rest of the SF history (SFH) and physical parameters we used the median values.

The fitting result depends on the observational data provided to the code as an input, which includes the observed fluxes and the associated observational uncertainties. Since the GAMA fluxes range from UV to FIR, the SED fitting estimates are reliable and well constrained. For each parameter, the median of the resultant probability density function is considered the best estimate of that parameter. Furthermore, the confidence interval is the 16th–84th percentile range (da Cunha et al. 2008; Baldry et al. 2018). For properties produced by the MAGPHYS

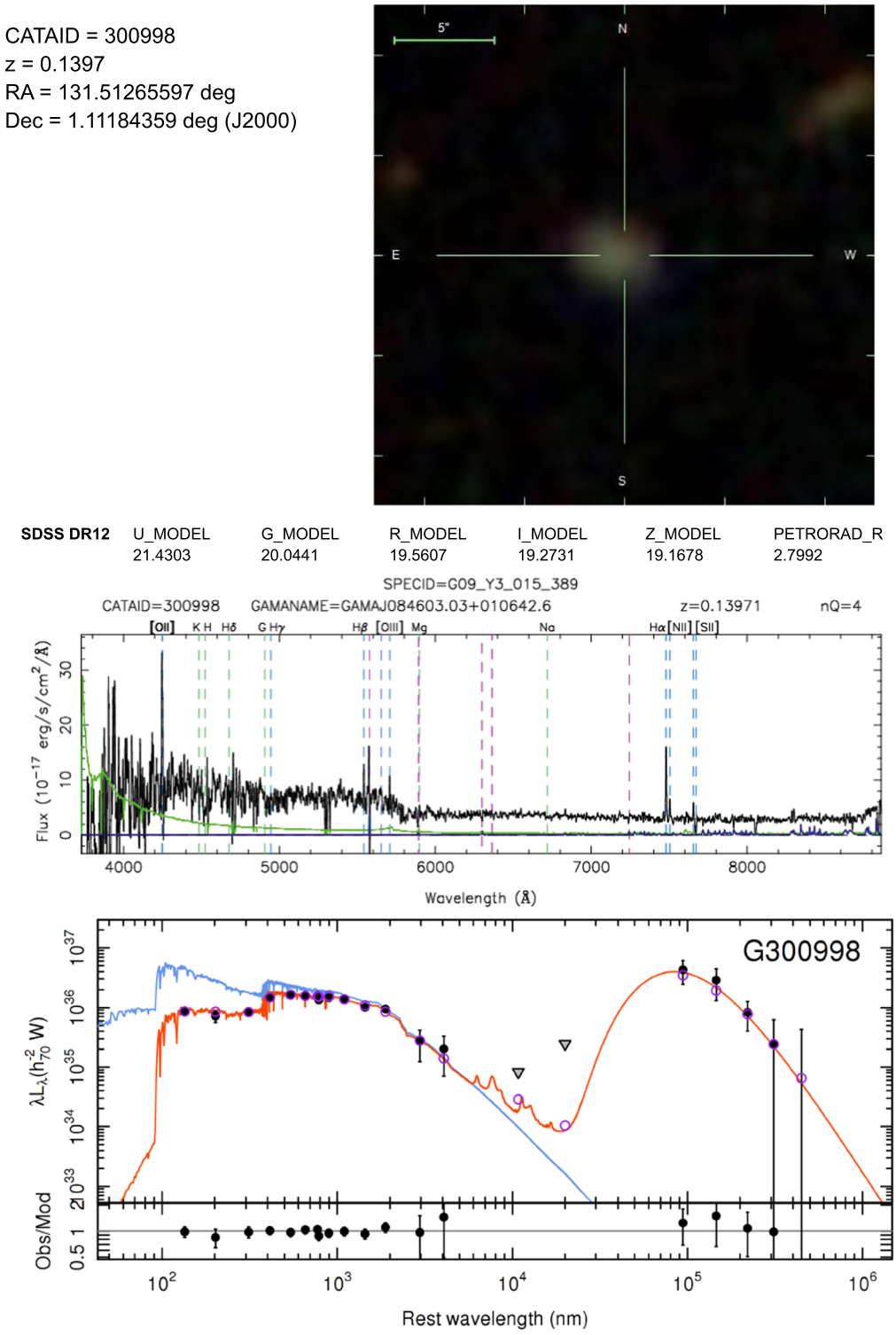

Figure 5. Quasar neighboring galaxy example. Top: postage stamp image of GAMA galaxy 300998 (GAMA Survey Image Viewer tool). Middle: spectrum (black line) and error (green line). Bottom: MAGPHYS fit (orange line) to data (filled dots and gray triangles for upper limits), with residuals underneath. Open magenta circles show the predicted photometry from the model. The blue line is a MAGPHYS model with no internal dust correction.

SED fitting code, we also report the uncertainties using the 16-50–84 percentile method. We compute for each neighbor the difference between the 50th (aka median) and 16th percentiles, and then take the median of these differences for all neighbors to be the typical lower uncertainty bound ($\widetilde{\Delta}_{16}$). For the typical upper uncertainty bound, the same calculation is done using the difference between the 84th and 50th percentiles ($\widetilde{\Delta}_{84}$).

3. Results

Since mergers are more likely in denser environments and SF bursts accompany simulated interactions (Di Matteo et al. 2005; Hopkins et al. 2006; Blandford et al. 2019), this study looks at the number counts and physical properties of galaxies in the vicinity of quasars (and matched inactive galaxies),

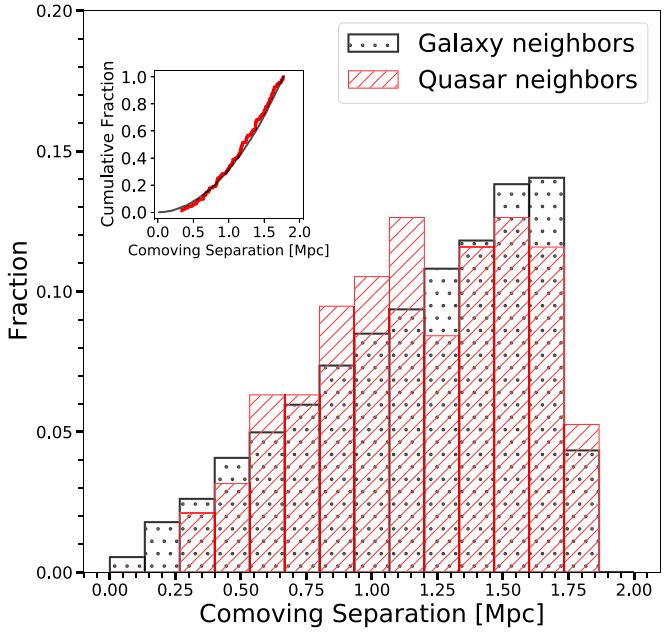

Figure 6. Comoving separation distributions of neighboring galaxies (quasar neighbors in red hatched bars, comparison galaxy neighbors in black dotted bars). The inset shows the empirical cumulative distribution function (eCDF; Seabold & Perktold 2010), quasar neighbors in red solid line, and comparison galaxy neighbors in black.

checking whether the observational data are consistent with the merger scenario. We first consider the counts of neighbors contained within a sphere of radius $R \sim 1.8$ Mpc for AGN host galaxies and the average counts of neighbors for galaxies in the comparison sample of matched inactive galaxies. For quasar host galaxies, 33.6% (69 out of 205) had at least one neighbor compared to $31.7\% \pm 3.3\%$ of the matched comparison galaxies on average. When considering only objects with neighbors, we find that for quasar host galaxies $68.1\% \pm 9.9\%$ had one neighbor, $26.0\% \pm 6.1\%$ had two, and $5.7\% \pm 2.8\%$ had three; while for the matched inactive galaxies respectively $77.6\% \pm 5.3\%$, $17.8\% \pm 4.9\%$, and $3.5\% \pm 2.1\%$. We find no significant difference in the fractions of neighbors for AGN hosts and inactive galaxies as would be expected if AGN hosts occupied denser environments. Additionally, Figure 6 shows the distributions of comoving separations for the neighboring galaxies of quasars and matched inactive galaxies. The comoving separations were derived following Lindsay et al. (2014) method. The KS test results in no significant difference between the two populations (Table 1), unlike what would be expected if AGNs were preferentially triggered by mergers. Therefore this suggests that there is no strong merger–AGN connection. For reasons of clarity and brevity, all subsequent figures in this section are shown in the Appendix; Table 1 points to these figures.

We then compare the distributions of several derived parameters for neighbors of AGN and our comparison sample of inactive galaxies. Figure 11 shows the distribution of Sérsic indices for neighbors of AGN hosts and for those of inactive galaxies. The mean values of both populations are similar ($n = 2.4 \pm 1.7$ for quasar neighbors, and $n = 2.6 \pm 2.6$ for comparison galaxy neighbors). The KS test does not reveal any significant statistical difference between the two samples.

Colors are shown here for comparison with other studies, although more detailed information on the properties of stellar populations is provided by GAMA's estimates of SFH. We have considered typical colors sensitive to age and metallicity such as $u - r$, $g - r$, $NUV - r$ (in AB system of magnitudes, Figures 12–14, respectively). Again there are no significant statistical differences between the distribution of galaxy colors for neighbors of AGN hosts and those of inactive galaxies. The color–magnitude plots show that the quasar neighbors and comparison galaxy neighbors populate the same areas.

Information on SFRs (Figure 15(a)); sSFRs (Figure 15(b)); SFRs averaged over 10, 100, 1000, and 2000 Myr (Figure 16); as well as the SF timescale (Figure 17(a)); time since the last burst of SF ended (Figure 17(b)); stellar masses (Figure 18(a)) and dust masses (Figure 18(b)), amount of stellar mass formed over time (Figure 19); ages (Figure 20(a)); and metallicities (Figure 20(b)) are derived by GAMA using MAGPHYS code (da Cunha et al. 2008; da Cunha & Charlot 2011). KS tests in no case indicate any significant difference in the properties of galaxies that are AGN neighbors or neighbors of inactive galaxies (Table 1).

Because the KS tests are sensitive to the bulk of the distributions and less to the wings, additionally an alternative test, the two-sample AD test (Scholz & Stephens 1987) of similarity was used. The AD test agreed with the KS test in all but two properties. The AD test for the fraction of mass formed in bursts over the last 10 and 100 Myr showed marginal difference.

3.1. Star Formation and Environment

We further investigate whether quasar neighbors are more similar to neighbors around star-forming galaxies (SFGs) or quiescent galaxies. We crudely split the sample of matched galaxies into two groups: SFGs and quiescent galaxies (Figure 7). SFGs have a tight correlation between the sSFR versus their stellar mass, known as the main sequence (MS; e.g., Noeske et al. 2007). To define the passive galaxies, we adopt a sSFR limit of $\log(\mathrm{sSFR}) = -10.8$ yr^{-1}, guided by the obvious double-peak nature of the sSFR distribution of the galaxies. We consider all galaxies either star-forming or passive, disregarding (for simplicity) the intermediate (aka "green valley") objects (Vulcani et al. 2015; Davies et al. 2016). For the SFGs, $\log(\mathrm{sSFR}) \geqslant -10.8$ yr^{-1}. For passive galaxies, $\log(\mathrm{sSFR}) < -10.8$ yr^{-1}. The median redshift of the SFGs is $z \sim 0.25$.

Then, we identify the neighbors of each subgroup. We compare the quasar sample of neighbors to the neighbors of each subgroup of comparison galaxies. All KS tests showed that both populations belong to the same parent distribution.

3.2. Stellar Mass and Environment

To check whether the environment effect depends on stellar mass, we divided our sample of quasars (and comparison galaxies) into two mass bins: low mass ($M_\star < 10^{10.5}\ M_\odot$) and high mass ($M_\star \geqslant 10^{10.5}\ M_\odot$), adopting the massive galaxy definition from Taylor et al. (2011). We used the stellar masses from MagPhys DMU. Also, we note that GAMA provides a more complete census of low-redshift galaxy population than the SDSS, especially for massive galaxies (Taylor et al. 2011). We checked that the redshift distribution is similar for both subsamples (low and high mass) between quasar neighbors and comparison galaxy neighbors by running a two-sample KS test.

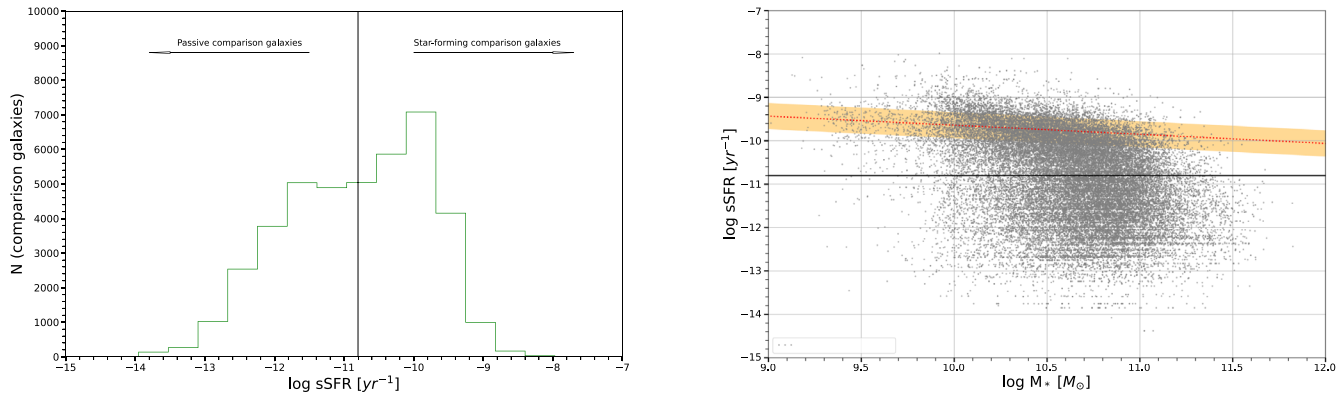

Figure 7. (a) sSFR distribution of comparison galaxies. The sSFR cutoff is shown by a black line. (b) SSFR vs. stellar mass for all comparison galaxies. We adopt the log(sSFR)$= -10.8$ yr^{-1} as the cutoff to define the SFGs (black solid line). For reference, we put the MS relation from literature (Ilbert et al. 2015), based on the median value of redshift for all star-forming comparison galaxies (red dashed line). The shaded area shows the typical 1σ dispersion (0.3 dex) for sSFR (Katsianis et al. 2019).

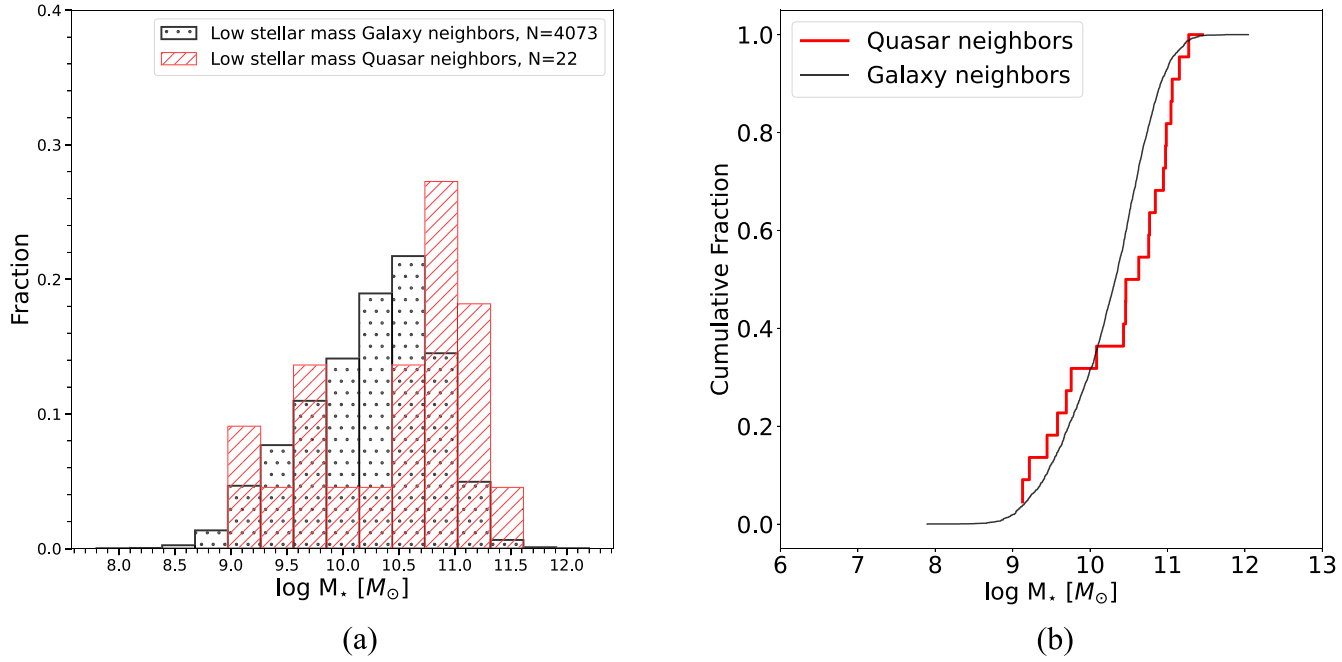

Figure 8. (a) Stellar mass distribution of neighbors around low-mass quasars and low-mass comparison galaxies. (b) KS test result. The eCDF, quasar neighbors in red solid line, and comparison galaxy neighbors in black.

We next compared the neighbors of low-mass quasars to the neighbors of low-mass comparison galaxies. Only in one instance, the KS test suggested that there are differences between the two populations—the stellar mass of neighbors (Figure 8). In the case of low-mass quasars, their neighbors do not have as many intermediate-mass galaxies, when compared to the low-mass comparison galaxies. This result is based on a small number of low-mass quasar neighbors, but if it is valid, then the absence of intermediate-mass companions suggests merger activity (Yue et al. 2019). The same analysis was done for the case of high-mass subsamples; however the KS test results were in favor of the hypothesis that high-mass quasar neighbors and high-mass comparison galaxy neighbors come from the same parent distribution.

4. Discussion

We have investigated the properties of neighbors of AGN host galaxies and a comparable sample of inactive galaxies matched in both mass and redshift within the same volume. Previous studies showed only a mild enhancement, if any, in the fraction of close companions associated with AGN host galaxies (Serber et al. 2006; Strand et al. 2008; Zhang et al. 2013); however the neighbors in the above-mentioned studies were selected using photometric data. Additionally, Strand et al. (2008), Zhang et al. (2013) lacked a comparison sample of inactive galaxies to isolate any effects due or related to the AGN from those of its environment. More recently, Bettoni et al. (2017, 2023), S21 used long-slit spectroscopy to measure

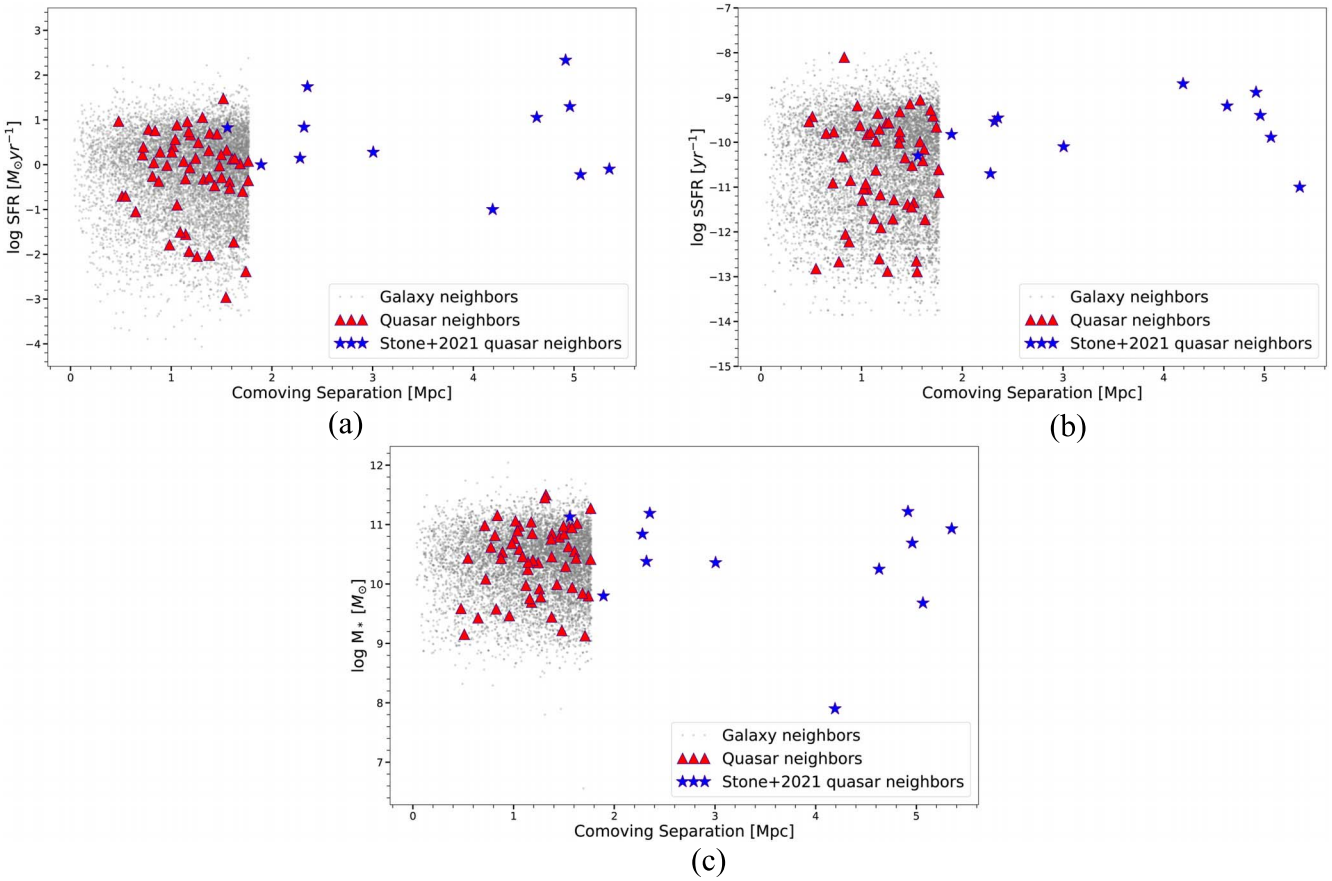

Figure 9. Correlation of (a) SFR vs. comoving separation of the neighboring galaxy from the quasar (or comparison galaxy), (b) sSFR vs. comoving separation, and (c) stellar mass vs. comoving separation. The comoving separation here is the distance from the central object (quasar or comparison galaxy). No differences are observed in these correlation plots between the neighbors of quasars and matched inactive galaxies.

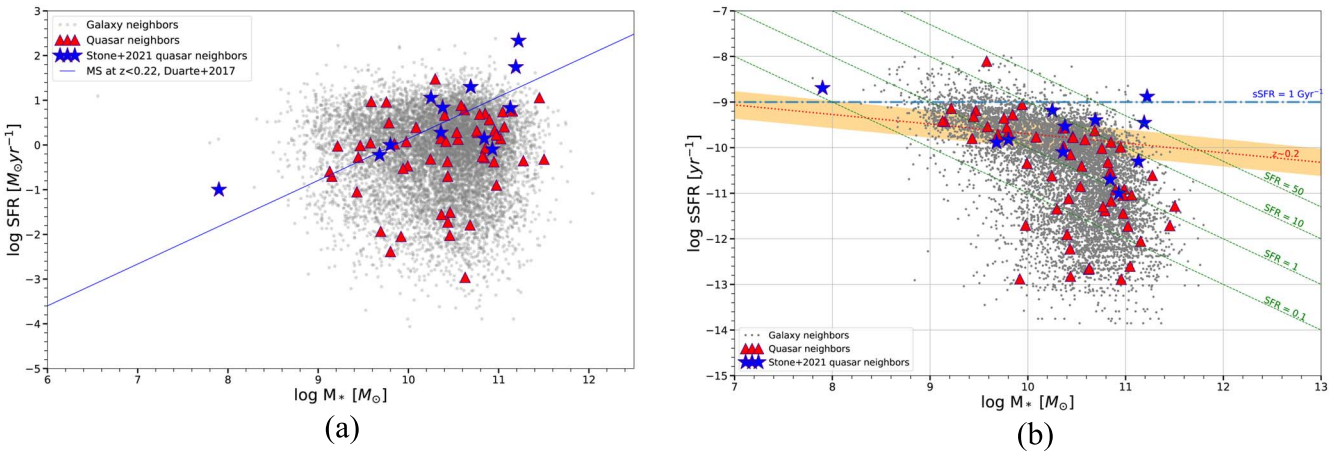

Figure 10. Correlations of mass with (a) SFR and (b) sSFR. Constant SFR ($M_\odot$ yr^{-1}) lines are green (dashed). The sSFR constant line is blue (dashed–dotted). The red dotted line is the MS relation from literature (Ilbert et al. 2015), using the median redshift of all comparison galaxy neighbors ($z \sim 0.3$). The shaded region around it is the typical 1σ dispersion (0.3 dex; Katsianis et al. 2019).

redshifts (and SF properties from emission lines) for galaxies projected near low-redshift ($z \lesssim 0.5$) AGN.

For the low-luminosity nearby quasars ($z < 0.5$, $\log(M_\star/M_\odot) < 11.5$), based on spectroscopic redshifts, our findings are consistent with recent results from Karhunen et al. (2014), Bettoni et al. (2015), and W22 who showed that AGN host galaxies occupy environments similar to those of a comparison sample matched in stellar mass and redshift, implying that the local galaxy environment provides little contribution to the AGN activity. The situation may, however, be different for brighter AGN and higher-redshift galaxies (e.g., Yue et al. 2019). Moreover, rich clusters are absent in GAMA regions, although the typical environment of galaxies (including quasar host galaxies as shown by W22) resembles that of a moderately rich group: AGN activity has a higher impact on the physical properties of neighbors in less massive objects.

One caveat is that our sample consists of unobscured quasars. Within the unification theory framework (Antonucci 1993; Urry & Padovani 1995), the unobscured quasars are expected to have the same properties as obscured quasars (as they evolve into each other). However, because some results suggest that obscured quasars are distinct objects, it is possible that their neighborhoods also differ from those of the unobscured quasars considered in this study.

The nature of neighboring galaxies may offer clues as to the nature of the AGN host galaxy (whose properties are often difficult to measure because of contamination from the bright nucleus) and to the effect of the AGN on its environment (e.g., where jets interact with the surrounding intergalactic medium, especially in denser environments, as in Martin-Navarro et al. 2021). The quasar hosts in our sample have various morphologies and SFR, as can be gleaned from few examples in Figures 3 and 4.

We find that there is no evidence of any significant difference between the neighbors of AGN host galaxies and those of the mass- and redshift-matched sample of inactive galaxies, in terms of morphology, current SFRs, SFH indicators, and age. This suggests that AGN host galaxies will also have very similar properties to those of inactive galaxies (in agreement with studies of quasar host galaxies at intermediate redshifts by Alam et al. 2021); similarly that the AGN activity also has little influence on the properties of its neighbors, although this may occur in environments where the intergalactic medium is denser (Dressler 1980). Figure 9 shows this particularly well, where we find that the sSFR of the neighbors of the AGN hosts does not depend on distance from the galaxy and follows the same distribution as for neighbors of inactive galaxies.

This is in agreement with earlier results from Villarroel (2012), although Coldwell & Lambas (2003, 2006) claimed an excess of SFGs within 1 Mpc of AGN. Neither do we see evidence that AGN hosts have more massive neighbors, unlike the trend claimed by Yue et al. (2019), albeit at a higher redshift.

We also explore the correlations of stellar mass and SFR for the neighbors (Figure 10(a)). The SFGs form a distinct sequence (MS) in the SFR (sSFR) versus $M_\star$ plane at a given redshift (Noeske et al. 2007; Kennicutt & Evans 2012). In our sample of low-redshift quasar and galaxy neighbors, the sSFR versus stellar mass plot (Figure 10(b)) shows that galaxies with lower stellar mass form stars at a higher rate as compared to more massive galaxies, as expected (e.g., Schreiber et al. 2016; Abdurro'uf & Akiyama 2017). We plot the MS relation from literature for low-redshift SFGs for reference in the log(SFR) versus log$M_\star$ plane (Duarte Puertas et al. 2017) and in the log(sSFR) versus log$M_\star$ plane (Ilbert et al. 2015). The shaded region in Figure 10(b)) shows the 1σ dispersion of sSFR. Most of the galaxy neighbors and quasar neighbors conform to the definition of SFG to some degree. Conversely, none of the neighboring galaxies in quasar fields have SFR larger than 50 $M_\odot$ yr^{-1}, which is against the scenario where mergers boost very high levels of SFR in AGN interactions.

Simulations in the scenarios where quasar activity is induced by mergers indicate starburst-like activity in the companion galaxies as well as the host. However, in our study, we do not observe any enhancement of SFR in the quasar companions relative to the neighbors of comparison galaxies. Further, we do not see any evidence that the neighbors closer to the quasar have higher SFR. While it is possible that the SF activity peaks on a shorter timescale, given our large number of quasars and their neighbors, our results are robust. Even when quasar companion samples are compared against only companions of the star-forming comparison galaxies or of only quiescent comparison galaxies, the SFR-related properties do not show any statistically significant difference.

These results suggest that at least at low-redshift AGN activity is not triggered by mergers and does not strongly depend on the environment. If secular processes are responsible, AGN are therefore a random occurrence in the lifetime of galaxies, and the correlations between galaxy properties and SMBH masses may occur via a random walk process (Jahnke & Maccio 2011). This is consistent with the recent simulations by Draper & Ballantyne (2012) showing that at lower redshifts processes other than mergers and interactions are the dominant AGN triggering mechanism. On the other hand, our results disagree with the conclusions of Gao et al. (2020), where merger fractions are higher in AGN than in non-AGN, although this may be explained by their inclusion of AGN selected in the mid-infrared, where merger rates seem to be consistently higher. In contrast, Silva et al. (2021) found that AGN fraction is similar in mergers and nonmergers. The existence of a merger–AGN connection remains a controversial issue.

5. Conclusions

We have studied the properties and environments of galaxies neighboring 205 low-redshift Type I (unobscured) AGN and a comparable sample of inactive galaxies, drawn from the GAMA survey in order to assess whether AGN hosts lie in different close environments and how they affect their neighbors. We found no evidence of any significant difference in the properties (morphology, colors, SFR, SFH, stellar mass, dust mass, age, and metallicity) of galaxies surrounding AGN hosts compared to those of inactive galaxies matched in mass and redshift and within the same volume. We explored the dependence of the environment effect on stellar mass and SF. Overall, our results suggest that the properties of galaxies around quasars are not influenced by the quasar activity. We conclude that AGN activity is more likely to be triggered by internal or secular processes, with major mergers playing only a minor role.

M.B.S. acknowledges useful discussion on galaxy clustering with Maret Einasto. M.B.S. acknowledges the Finnish Cultural Foundation grant No. 00220968 and Finnish Centre for Astronomy with ESO grant. M.B.S. and J.K. acknowledge financial support from the Academy of Finland, grant 311438.

GAMA is a joint European-Australasian project based around a spectroscopic campaign using the Anglo-Australian Telescope. The GAMA input catalog is based on data taken from the Sloan Digital Sky Survey and the UKIRT Infrared Deep Sky Survey. Complementary imaging of the GAMA regions is being obtained by a number of independent survey programmes including GALEX Medium Imaging Survey (MIS), VLT Survey Telescope (VST) KiDS, VISTA VIKING, Wide-field Infrared Survey Explorer (WISE), Herschel-ATLAS, GMRT, and ASKAP providing UV to radio coverage. GAMA is funded by the STFC (UK), the Australian Research Council (ARC, Australia), the Australian Astronomical Observatory (AAO), and the participating institutions. The GAMA website is http://www.gama-survey.org/.

This research has made use of the NASA/IPAC Extragalactic Database (NED), which is operated by the Jet Propulsion Laboratory, California Institute of Technology, under contract with the National Aeronautics and Space

Administration. This research made use of the NASA's Astrophysics Data System Bibliographic Services, Astrobetter blog and wiki, and cosmology calculator by Wright (2006). This research has made use of the SIMBAD database, operated at the Strasbourg Astronomical Data Center (CDS), Strasbourg, France. This research made use of code from Stone (2017). This research has made use of the VizieR catalog access tool, CDS, Strasbourg, France (DOI: 10.26093/cds/vizier). The original description of the VizieR service was published in 2000, AAS 143, 23.

Facility: Anglo-Australian Telescope (AAT).

Software: Astropy (Astropy Collaboration et al. 2013, 2018), NUMPY (Harris et al. 2020), SCIPY (Virtanen et al. 2020), MATPLOTLIB (Hunter 2007).

Appendix
Distributions of Properties

From here we show the distribution plots for the properties considered in this work, as mentioned in Table 1: morphology (Figure 11), colors (Figures 12–14), SFH (Figures 15–17), and physical parameters (Figures 18–20). We used the KS test to compare the neighbors of quasars with the neighbors of matched inactive galaxies, finding no statistically significant differences in each case.

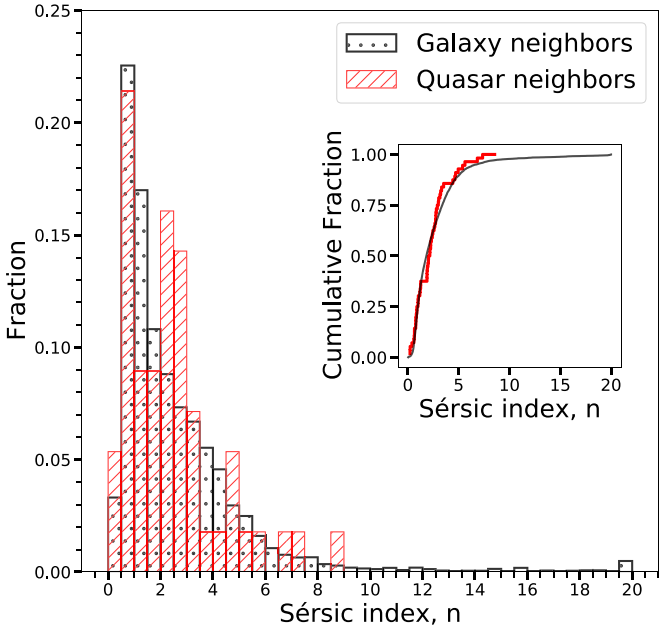

Figure 11. Sérsic index (quasar neighbors in red hatched bars, comparison galaxy neighbors in black dotted bars). The inset shows the eCDF, quasar neighbors in red solid line, and comparison galaxy neighbors in black. Median error for Sérsic index values from GAMA is ∼0.14 both for quasar neighbors and for comparison galaxy neighbors.

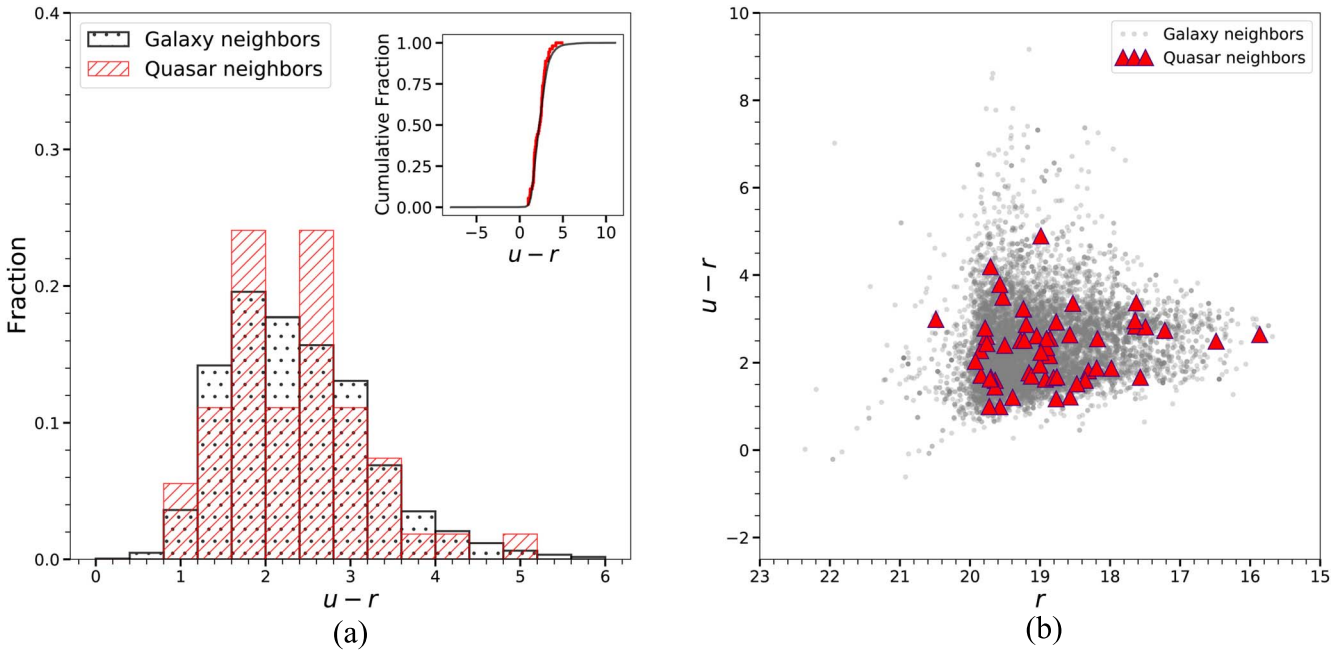

Figure 12. (a) SDSS $u - r$ color (quasar neighbors in red hatched bars, comparison galaxy neighbors in black dotted bars). The inset shows the eCDF, quasar neighbors in red solid line, and comparison galaxy neighbors in black. (b) Color–magnitude plot. Median error for SDSS u–r color from GAMA is ∼0.34 for quasar neighbors and ∼0.46 for comparison galaxy neighbors. Median error for SDSS r is ∼0.03 for both quasar neighbors and for comparison galaxy neighbors. To propagate the error, standard uncertainty propagation rules were used.

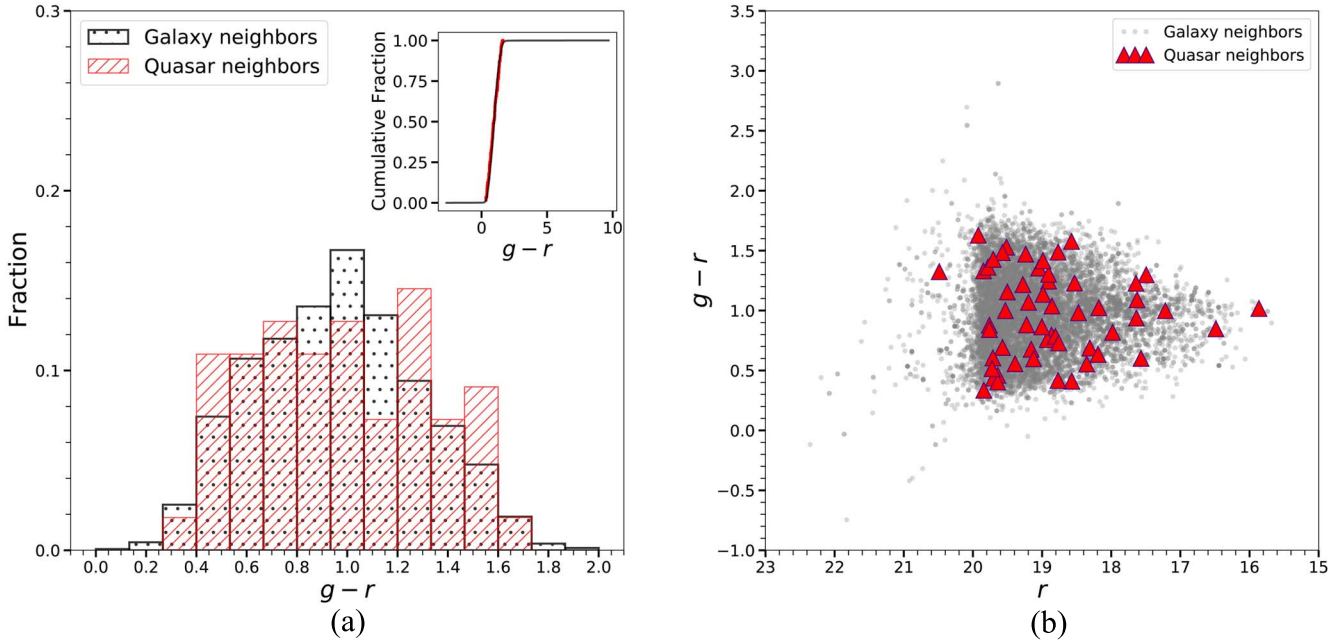

Figure 13. (a) SDSS $g - r$ color (quasar neighbors in red hatched bars, comparison galaxy neighbors in black dotted bars). The inset shows the eCDF, quasar neighbors in red solid line, and comparison galaxy neighbors in black. (b) Color–magnitude plot. Median error for SDSS g–r color from GAMA is ∼0.05 for quasar neighbors and ∼0.06 for comparison galaxy neighbors. Median error for SDSS r is ∼0.03 for both quasar neighbors and for comparison galaxy neighbors. To propagate the error, standard uncertainty propagation rules were used.

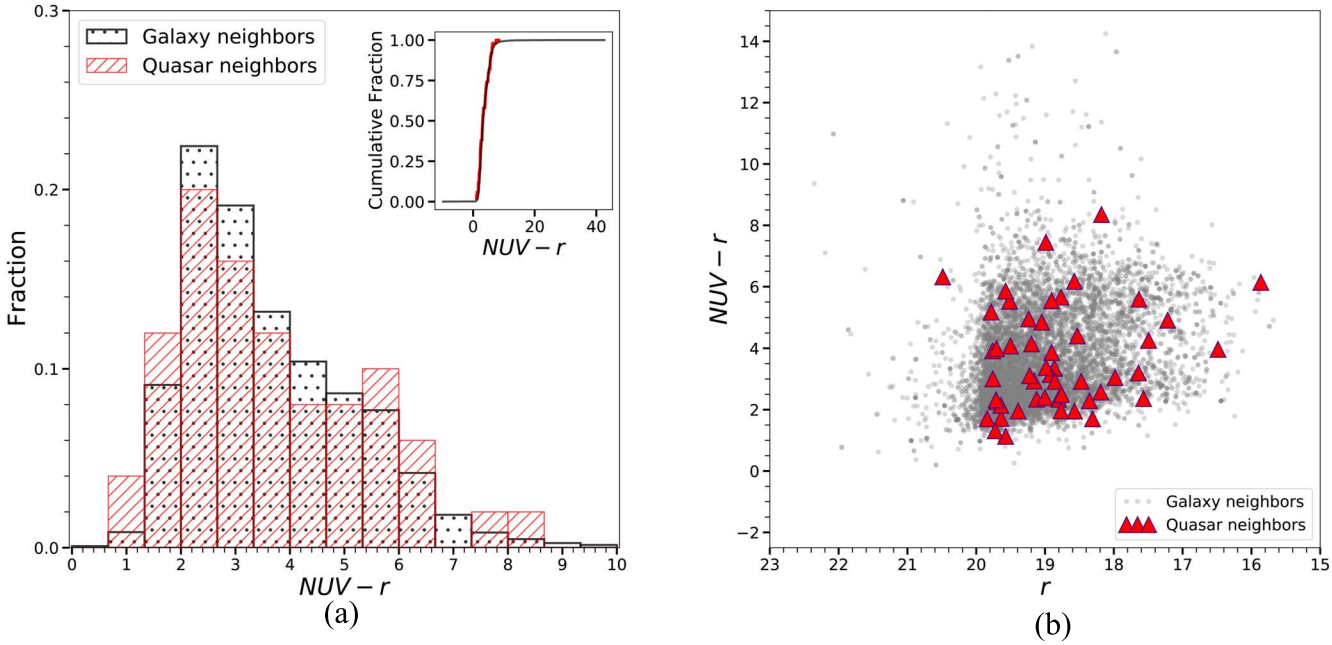

Figure 14. (a) GALEX NUV–SDSS r color (quasar neighbors in red hatched bars, comparison galaxy neighbors in black dotted bars). The inset shows the eCDF, quasar neighbors in red solid line, and comparison galaxy neighbors in black. (b) Color–magnitude plot. Median error for NUV–SDSS r color from GAMA is ∼2.1 for quasar neighbors and ∼2.4 for comparison galaxy neighbors. Median error for r is ∼0.03 for both quasar neighbors and for comparison galaxy neighbors. To propagate the error, standard uncertainty propagation rules were used.

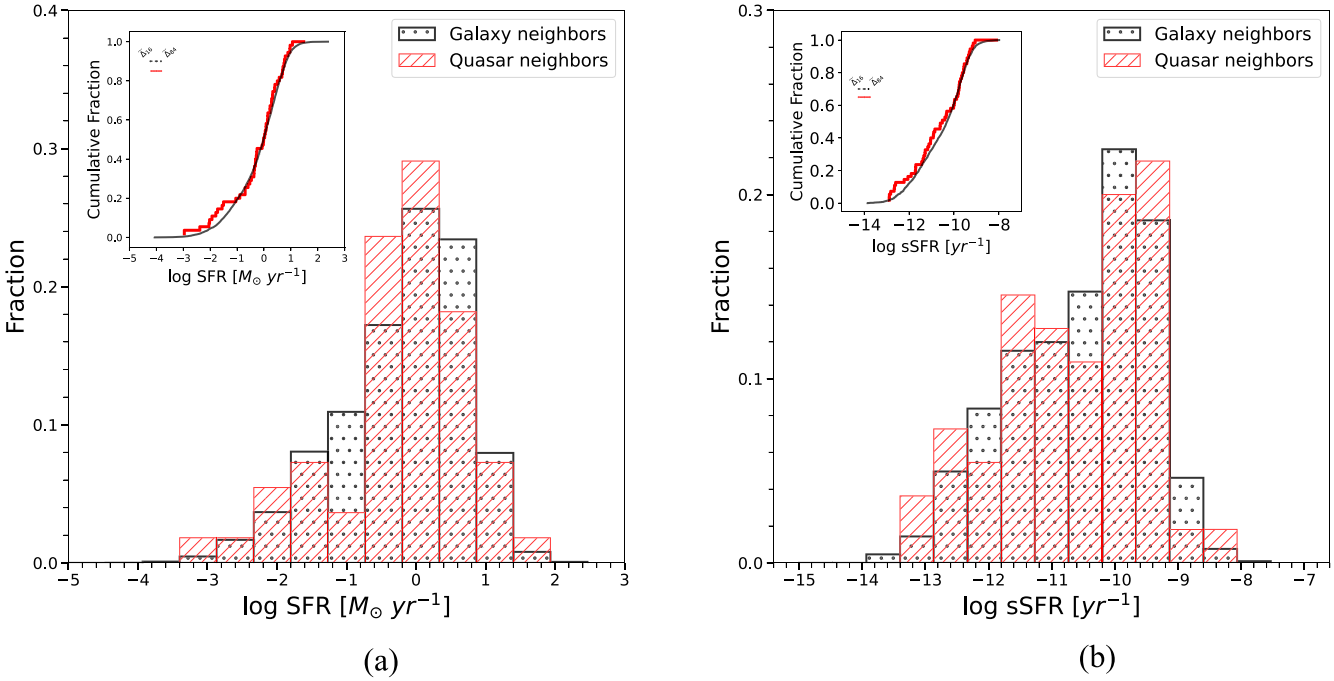

Figure 15. (a) SFR. (b) sSFR (quasar neighbors in red hatched bars, comparison galaxy neighbors in black dotted bars). The inset shows the eCDF, quasar neighbors in red solid line, and comparison galaxy neighbors in black. The typical uncertainty is represented by the median values of 16th and 84th percentiles.

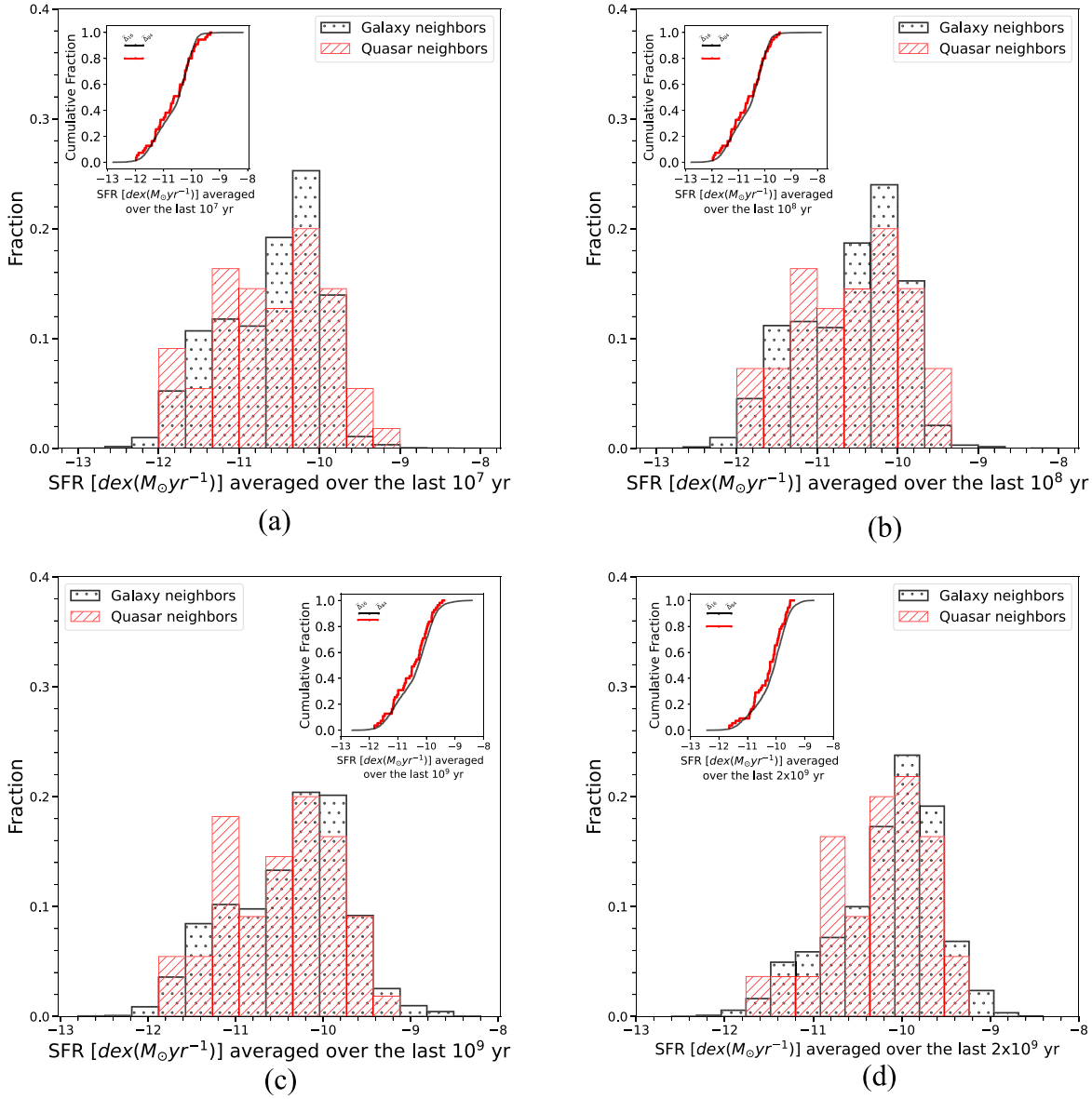

Figure 16. Median SFR averaged over the past 10^7, 10^8, 10^9, 2×10^9 yr (quasar neighbors in red hatched bars, comparison galaxy neighbors in black dotted bars). The inset shows the eCDF, quasar neighbors in red solid line, and comparison galaxy neighbors in black. The typical uncertainty is represented by the median values of 16th and 84th percentiles.

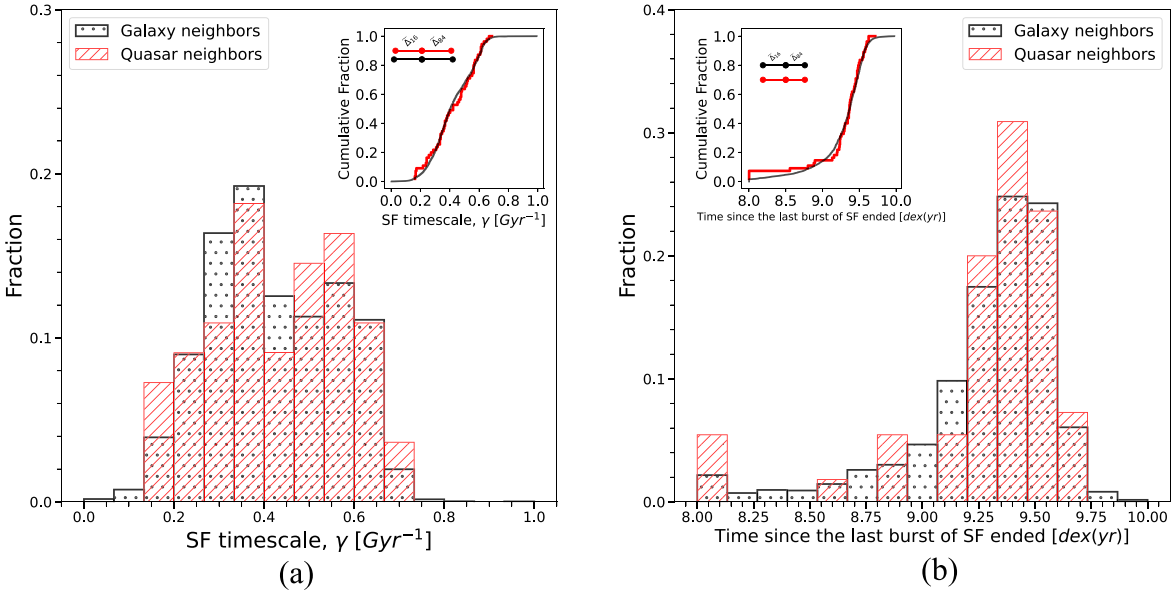

Figure 17. (a) Median SF timescale. (b) Median time since the last burst of SF ended (quasar neighbors in red hatched bars, comparison galaxy neighbors in black dotted bars). The inset shows the eCDF, quasar neighbors in red solid line, and comparison galaxy neighbors in black. The typical uncertainty is represented by the median values of 16th and 84th percentiles.

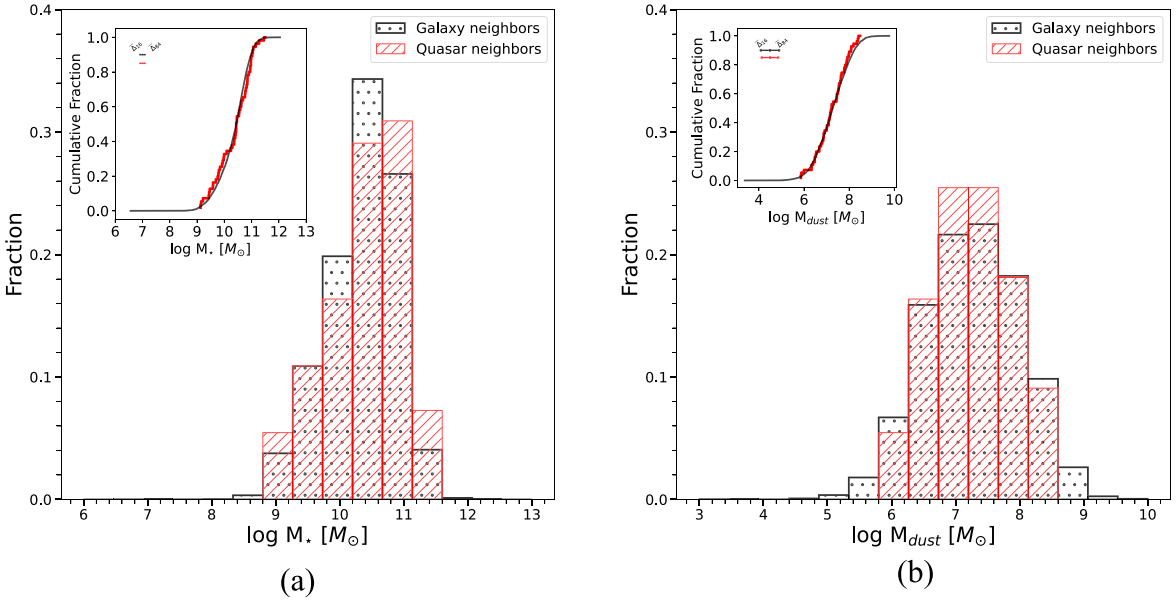

Figure 18. (a) Stellar mass. (b) Dust mass (quasar neighbors in red hatched bars, comparison galaxy neighbors in black dotted bars). The inset shows the eCDF, quasar neighbors in red solid line, and comparison galaxy neighbors in black. The typical uncertainty is represented by the median values of 16th and 84th percentiles.

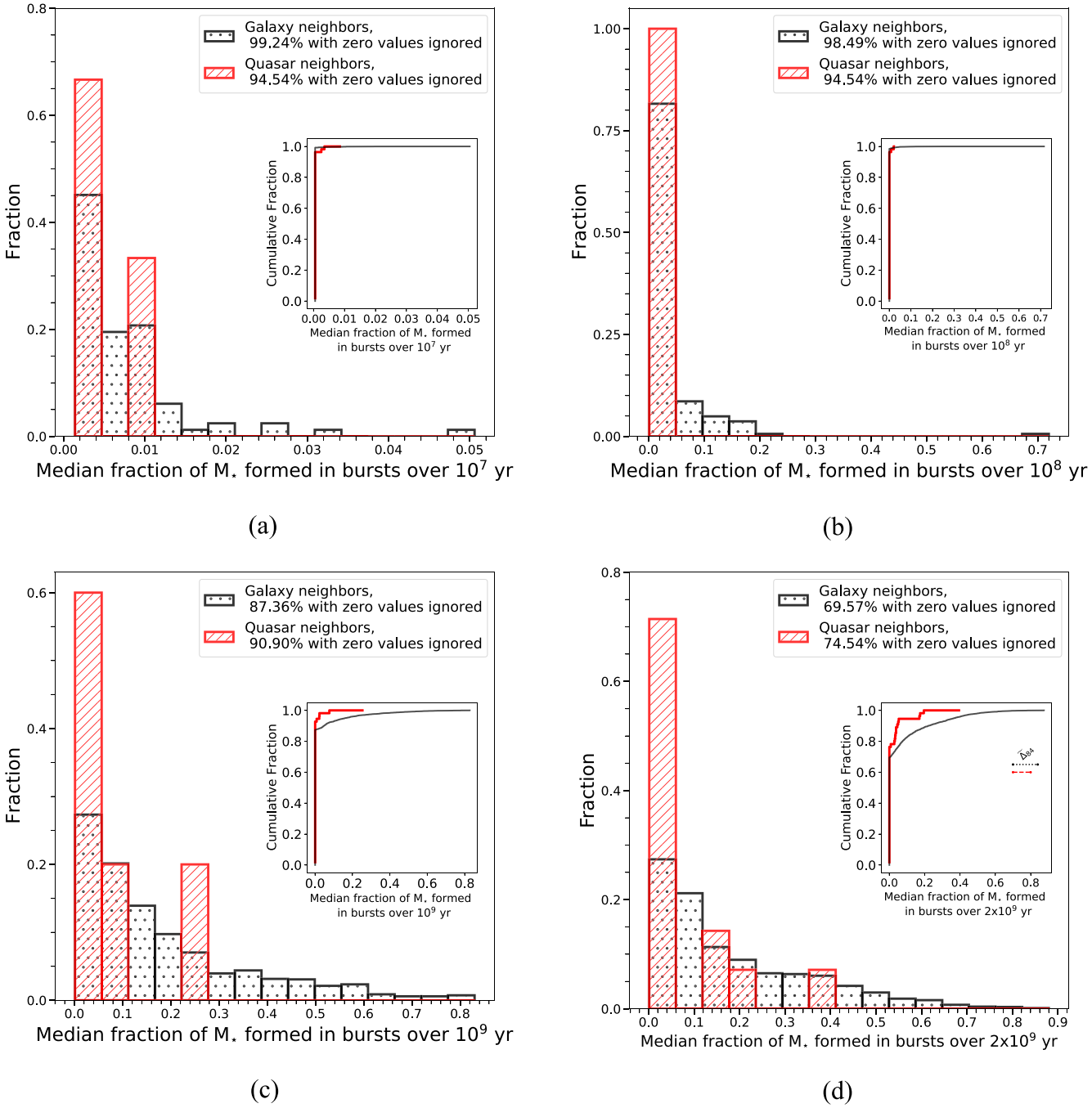

Figure 19. Median fraction of stellar mass formed in bursts over the past 10^7, 10^8, 10^9, 2×10^9 yr. This is the effective $M_\star$ accounting for the mass returned to the interstellar medium (quasar neighbors in red hatched bars, comparison galaxy neighbors in black dotted bars). The inset shows the eCDF, quasar neighbors in red solid line, and comparison galaxy neighbors in black. The typical uncertainty is represented by the median values of 16th and 84th percentiles. The properties in panels (a), (b), and (c) had zero-value uncertainties, while the property in panel (d) had a zero-value lower bound uncertainty.

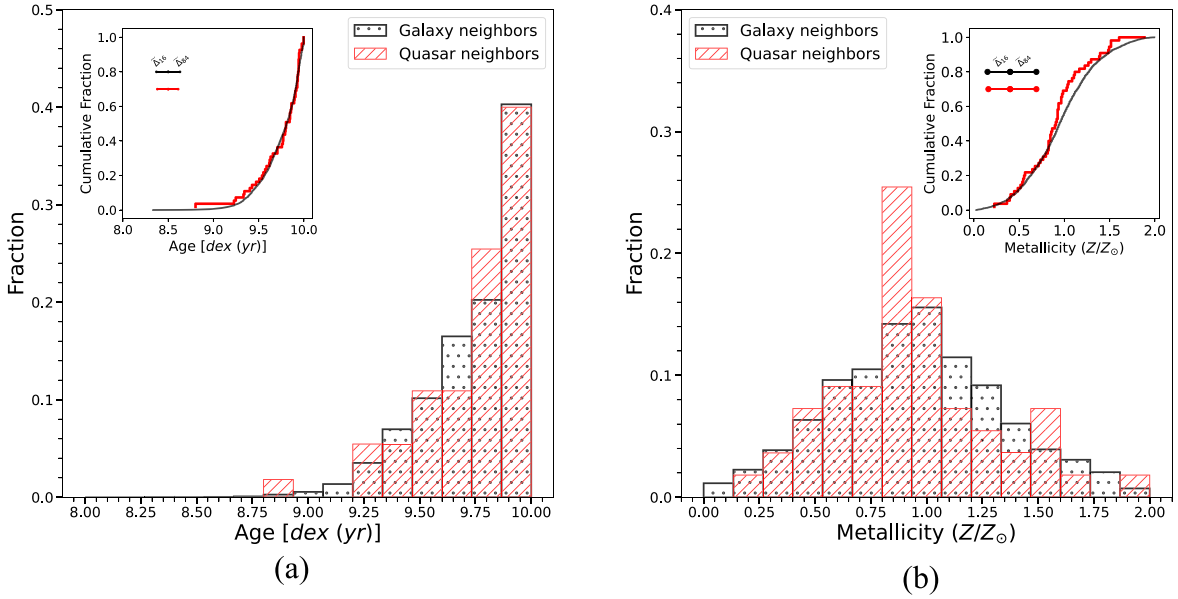

Figure 20. (a) Age. (b) Metallicity (quasar neighbors in red hatched bars, comparison galaxy neighbors in black dotted bars). The inset shows the eCDF, quasar neighbors in red solid line, and comparison galaxy neighbors in black. The typical uncertainty is represented by the median values of 16th and 84th percentiles.

ORCID iDs

Maria B. Stone https://orcid.org/0000-0002-2931-0593
Clare F. Wethers https://orcid.org/0000-0002-7135-2842
Roberto de Propris https://orcid.org/0000-0003-1455-7339
Jari Kotilainen https://orcid.org/0000-0003-0133-7644
Nischal Acharya https://orcid.org/0000-0001-9738-3594
Benne W. Holwerda https://orcid.org/0000-0002-4884-6756
Jonathan Loveday https://orcid.org/0000-0001-5290-8940
Steven Phillipps https://orcid.org/0000-0001-5991-3486

References

Abdurro'uf, & Akiyama, M. 2017, MNRAS, 469, 2806
Ahn, C. P., Alexandroff, R., Allende Prieto, C., et al. 2014, ApJS, 211, 17
Ahumada, R., Prieto, C. A., Almeida, A., et al. 2020, ApJS, 249, 3
Alam, S., Ross, N. P., Eftekharzadeh, S., et al. 2021, MNRAS, 504, 857
Alexander, D. M., & Hickox, R. C. 2012, NewAR, 56, 93
Annis, J., Soares-Santos, M., Strauss, M. A., et al. 2014, ApJ, 794, 120
Antonucci, R. 1993, ARA&A, 31, 473
Astropy Collaboration, Price-Whelan, A. M., Sipőcz, B. M., et al. 2018, AJ, 156, 123
Astropy Collaboration, Robitaille, T. P., Tollerud, E. J., et al. 2013, A&A, 558, A33
Baldry, I. K., Alpaslan, M., Bauer, A. E., et al. 2014, MNRAS, 441, 2440
Baldry, I. K., Liske, J., Brown, M. J. I., et al. 2018, MNRAS, 474, 3875
Barnes, J. E., & Hernquist, L. E. 1991, ApJL, 370, L65
Bettoni, D., Falomo, R., Kotilainen, J. K., & Karhunen, K. 2017, MNRAS, 466, 3600
Bettoni, D., Falomo, R., Kotilainen, J. K., Karhunen, K., & Uslenghi, M. 2015, MNRAS, 454, 4103
Bettoni, D., Falomo, R., Paiano, S., Kotilainen, J. K., & Stone, M. B. 2023, MNRAS, 519, 2929
Blandford, R., Meier, D., & Readhead, A. 2019, ARA&A, 57, 467
Blumenthal, K. A., & Barnes, J. E. 2018, MNRAS, 479, 3952
Bruzual, G., & Charlot, S. 2003, MNRAS, 344, 1000
Carlberg, R. G., Yee, H. K. C., Ellingson, E., et al. 1996, ApJ, 462, 32
Carlberg, R. G., Yee, H. K. C., & Ellingson, E. 1997, ApJ, 478, 462
Cisternas, M., Jahnke, K., Inskip, K. J., et al. 2011, ApJ, 726, 57
Coldwell, G. V., & Lambas, D. G. 2003, MNRAS, 344, 156
Coldwell, G. V., & Lambas, D. G. 2006, MNRAS, 371, 786
da Cunha, E., & Charlot, S. 2011, MAGPHYS: Multi-wavelength Analysis of Galaxy Physical Properties, Astrophysics Source Code Library, ascl:1106.010
da Cunha, E., Charlot, S., & Elbaz, D. 2008, MNRAS, 388, 1595
Dashyan, G., Choi, E., Somerville, R. S., et al. 2019, MNRAS, 487, 5889
Davies, L. J. M., Robotham, A. S. G., Driver, S. P., et al. 2016, MNRAS, 455, 4013
De Propris, R., Baldry, I. K., Bland-Hawthorn, J., et al. 2014, MNRAS, 444, 2200
Debuhr, J., Quataert, E., & Ma, C.-P. 2011, MNRAS, 412, 1341
Di Matteo, T., Springel, V., & Hernquist, L. 2005, Natur, 433, 604
Draper, A. R., & Ballantyne, D. R. 2012, ApJ, 751, 72
Dressler, A. 1980, ApJ, 236, 351
Driver, S. P., Andrews, S. K., da Cunha, E., et al. 2018, MNRAS, 475, 2891
Driver, S. P., Bellstedt, S., Robotham, A. S. G., et al. 2022, MNRAS, 513, 439
Driver, S. P., Hill, D. T., Kelvin, L. S., et al. 2011, MNRAS, 413, 971
Driver, S. P., Wright, A. H., Andrews, S. K., et al. 2016, MNRAS, 455, 3911
Duarte Puertas, S., Vilchez, J. M., Iglesias-Páramo, J., et al. 2017, A&A, 599, A71
Fan, L., Han, Y., Fang, G., et al. 2016, ApJL, 822, L32
Gabor, J. M., Capelo, P. R., Volonteri, M., et al. 2016, A&A, 592, A62
Gao, F., Wang, L., Pearson, W. J., et al. 2020, A&A, 637, A94
Gattano, C., Andrei, A. H., Coelho, B., et al. 2018, A&A, 614, A140
Goulding, A. D., Greene, J. E., Bezanson, R., et al. 2018, PASJ, 70, S37
Gunn, J. E. 1979, in Active Galactic Nuclei, ed. C. Hazard & S. Mitton (Cambridge: Cambridge Univ. Press), 213
Harris, C. R., Millman, K. J., van der Walt, S. J., et al. 2020, Natur, 585, 357
Hayward, C. C., & Smith, D. J. B. 2015, MNRAS, 446, 1512
Hill, D. T., Kelvin, L. S., Driver, S. P., et al. 2011, MNRAS, 412, 765
Holwerda, B. W., Wu, J. F., Keel, W. C., et al. 2021, ApJ, 914, 142
Hopkins, P. F., & Hernquist, L. 2006, ApJS, 166, 1
Hopkins, P. F., Hernquist, L., Cox, T. J., et al. 2006, ApJS, 163, 1
Hopkins, P. F., & Quataert, E. 2010, MNRAS, 407, 1529
Hunt, L. K., De Looze, I., Boquien, M., et al. 2019, A&A, 621, A51
Hunter, J. D. 2007, CSE, 9, 90
Ilbert, O., Arnouts, S., Le Floc'h, E., et al. 2015, A&A, 579, A2
Jahnke, K., & Macciò, A. V. 2011, ApJ, 734, 92
Karhunen, K., Kotilainen, J. K., Falomo, R., & Bettoni, D. 2014, MNRAS, 441, 1802
Katsianis, A., Zheng, X., Gonzalez, V., et al. 2019, ApJ, 879, 11
Kelvin, L. S., Driver, S. P., Robotham, A. S. G., et al. 2012, MNRAS, 421, 1007
Kennicutt, R. C., & Evans, N. J. 2012, ARA&A, 50, 531
Kormendy, J., Fisher, D. B., Cornell, M. E., & Bender, R. 2009, ApJS, 182, 216
Kormendy, J., & Ho, L. C. 2013, ARA&A, 51, 511
Lietzen, H., Heinämäki, P., Nurmi, P., et al. 2011, A&A, 535, A21
Lindsay, S. N., Jarvis, M. J., Santos, M. G., et al. 2014, MNRAS, 440, 1527
Liske, J., Baldry, I. K., Driver, S. P., et al. 2015, MNRAS, 452, 2087
Lynden-Bell, D. 1969, Natur, 223, 690

Marian, V., Jahnke, K., Andika, I., et al. 2020, ApJ, 904, 79
Martin, D. C., Fanson, J., Schiminovich, D., et al. 2005, ApJL, 619, L1
Martín-Navarro, I., Burchett, J. N., & Mezcua, M. 2019, ApJL , 884, L45
Martín-Navarro, I., Burchett, J. N., Mezcua, M., & Scholz-Díaz, L. 2020, in Conrib. XIV.0 Sci. Meet. (virtual) Span. Astron. Soc. (SEA) (Barcelona: SEA), 58
Martin-Navarro, I., Pillepich, A., Nelson, D., et al. 2021, Natur, 594, 187
Martín-Navarro, I., Shankar, F., & Mezcua, M. 2022, MNRAS Lett., 513, L10
Molnár, D. C., Sargent, M. T., Elbaz, D., Papadopoulos, P. P., & Silk, J. 2017, MNRAS, 467, 586
Newton, R. D. A., & Kay, S. T. 2013, MNRAS, 434, 3606
Noeske, K. G., Weiner, B. J., Faber, S. M., et al. 2007, ApJL, 660, L43
Ochsenbein, F., Bauer, P., & Marcout, J. 2000, A&AS, 143, 23
Padovani, P. 2016, A&ARv, 24, 13
Peng, C. Y., Ho, L. C., Impey, C. D., & Rix, H.-W. 2002, AJ, 124, 266
Peng, C. Y., Ho, L. C., Impey, C. D., & Rix, H.-W. 2010, AJ, 139, 2097
Porqueres, N., Jasche, J., Enßlin, T. A., & Lavaux, G. 2018, A&A, 612, A31
Planck Collaboration, Aghanim, N., Akrami, Y., et al. 2020, A&A, 641, A6
Robotham, A. S. G., Driver, S. P., Davies, L. J. M., et al. 2014, MNRAS, 444, 3986
Sánchez, S. F., Avila-Reese, V., Hernandez-Toledo, H., et al. 2018, RMxAA, 54, 217
Sanders, D. B., Soifer, B. T., Elias, J. H., et al. 1988, ApJ, 325, 74
Schaye, J., Vecchia, C. D., Booth, C. M., et al. 2010, MNRAS, 402, 1536
Scholz, F. W., & Stephens, M. A. 1987, J. Am. Stat. Assoc., 82, 918
Schreiber, C., Elbaz, D., Pannella, M., et al. 2016, A&A, 589, A35
Seabold, S., & Perktold, J. 2010, in Proc. 9th Python Sci. Conf. (SciPy 2010), ed. S. van der Walt & J. Millman (Austin, TX: SciPy), 92
Serber, W., Bahcall, N., Ménard, B., & Richards, G. 2006, ApJ, 643, 68
Sérsic, J. L. 1968, Atlas de Galaxias Australes (Cordoba: Argentina: Observatorio Astronomico)
Shlosman, I., Frank, J., & Begelman, M. C. 1989, Natur, 338, 45
Silk, J., & Rees, M. J. 1998, A&A, 331, L1
Silva, A., Marchesini, D., Silverman, J. D., et al. 2021, ApJ, 909, 124
Smethurst, R. J., Simmons, B. D., Lintott, C. J., et al. 2021, MNRAS, 506, 3419
Stone, M. B. 2017, Master's thesis, San Jose State Univ., California
Stone, M. B., Bettoni, D., Falomo, R., et al. 2021, MNRAS, 501, 419
Strand, N. E., Brunner, R. J., & Myers, A. D. 2008, ApJ, 688, 180
Taylor, E. N., Hopkins, A. M., Baldry, I. K., et al. 2011, MNRAS, 418, 1587
Treister, E., Schawinski, K., Urry, C. M., & Simmons, B. D. 2012, ApJL, 758, L39
Tumlinson, J., Peeples, M. S., & Werk, J. K. 2017, ARA&A, 55, 389
Urry, C. M., & Padovani, P. 1995, PASP, 107, 803
Villarroel, B. 2012, A&A, 542, A72
Villforth, C., Hamilton, T., Pawlik, M. M., et al. 2017, MNRAS, 466, 812
Villforth, C., Herbst, H., Hamann, F., et al. 2019, MNRAS, 483, 2441
Virtanen, P., Gommers, R., Oliphant, T. E., et al. 2020, NatMe, 17, 261
Vulcani, B., Poggianti, B. M., Fritz, J., et al. 2015, ApJ, 798, 52
Wethers, C. F., Acharya, N., De Propris, R., et al. 2022, ApJ, 928, 192
Wright, A. H., Robotham, A. S. G., Bourne, N., et al. 2016, MNRAS, 460, 765
Wright, E. L. 2006, PASP, 118, 1711
Wurster, J., & Thacker, R. J. 2013, MNRAS, 431, 2513
Yue, M., Fan, X., Schindler, J.-T., McGreer, I. D., & Huang, Y.-H. 2019, ApJ, 883, 141
Zana, T., Gallerani, S., Carniani, S., et al. 2022, MNRAS, 513, 2118
Zhang, S., Wang, T., Wang, H., & Zhou, H. 2013, ApJ, 773, 175
Zhuang, M.-Y., & Ho, L. C. 2022, ApJ, 934, 130